The detailed dynamics of the Hadley Cell. Part 2: December to February

Article

Accepted Version

The detailed dynamics of the Hadley Cell. Part 2: December to February

B. J. Hoskins [a,b] and G.-Y. Yang [a,c]

a. Department of Meteorology, University of Reading, UK

b. Grantham Institute for Climate Change, Imperial College, London, UK

c. Climate Directorate, National Centre for Atmospheric Science, University of Reading, UK

Submitted to Journal of Climate

Revised in October

*Corresponding Author address:

Gui-Ying Yang

National Centre of Atmospheric Science,

and Department of Meteorology,

University of Reading, Earley Gate,

Reading RG6 6BB, UK

Email: g.y.yang@reading.ac.uk

Early Online Release: This preliminary version has been accepted for publication in *Journal of Climate*, may be fully cited, and has been assigned DOI 10.1175/JCLI-D-20-0504.1. The final typeset copyedited article will replace the EOR at the above DOI when it is published.

Abstract

This paper compliments an earlier paper on the June-August Hadley Cell by giving a detailed analysis of the December to February Hadley Cell as seen in a 30-year climatology of ERA-Interim data. The focus is on the dynamics of the upper branch of the Hadley Cell. There are significant differences between the Hadley Cells in the two solsticial seasons. These are particularly associated with the ITCZs staying north of the equator and with mean westerlies in the equatorial regions of the E Pacific and Atlantic in December to February. The latter enables Westward-moving Mixed Rossby Gravity waves to be slow moving in those regions and therefore respond strongly to upstream off-equatorial active convection. However, the main result is that in both seasons it is the regions and times of active convection that predominantly lead to upper tropospheric out-flows and structures that average to give the mean flow towards the winter pole, and the steady and transient fluxes of momentum and vorticity that balance the Coriolis terms. The response to active convection in preferred regions is shown by means of regressions on the data from the climatology and by synoptic examples from one season. Eddies with tropical origin are seen to be important in their own right and also in their interaction with higher latitude systems. There is support for the relevance of a new conceptual model of the Hadley Cell based on the sporadic nature of active tropical convection in time and space.

Accepted for publication in *Journal of Climate*. DOI 10.1175/JCLI-D-20-0504.1.

1. Introduction

The concept of the Hadley Cell (HC) in the zonally averaged view of the atmosphere is at the core of the traditional view of the general circulation of the atmosphere as discussed, for example, in Lorenz (1967). As reviewed by Held (2018), there have been contrasting views about the relative importance of tropical and midlatitude phenomena and processes for the existence, strength, and extent of the Earth's Hadley Cells and the strength of the upper tropospheric subtropical jets on their poleward flank. From the midlatitude perspective, Jeffreys (1926) raised the importance for the maintenance of the surface westerlies in midlatitudes of angular momentum transfers from the subtropics by midlatitude eddies. The early datasets for computation of momentum fluxes (e.g. Starr, 1948) were only for the extra-tropical region. Eady (1950) saw that, maintenance of thermal wind balance would require that the midlatitude eddy induced poleward momentum transfer in the upper troposphere must be accompanied by a Hadley Cell, though this is weak, as was shown for the life cycle of a baroclinic wave by Simmons and Hoskins (1978). As was quoted by Held (2018), baroclinic instability has also for many decades been seen as a limiter on the latitudinal extent of the Hadley Cell. In their axisymmetric simulations using a dynamical core, Davis and Birner (2019) found that the Hadley Cell only extended through the depth of the atmosphere to the lower boundary if they included significant viscosity or prescribed eddy driving. Schneider (2006), stressed the importance for the Hadley Cells of the extra-tropical eddies, and in subsequent years, the emphasis has often been on their strong, and even controlling, influence on the HC.

However, from the tropical perspective, the improvement of data availability permitted Starr et al (1970) to calculate momentum transport for the whole northern hemisphere and for the four seasons. In winter the upper tropospheric poleward momentum flux by transient eddies occurred started from the deep tropics, but there were indications of a

Accepted for publication in *Journal of Climate*. DOI 10.1175/JCLI-D-20-0504.1.

reversal of the direction of transport by both standing and transient eddies in the lowest latitudes. Rosen and Salstein (1980) also saw these features in their improved data sets, and they were discussed by Dima and Wallace (2003). Dima et al (2005) associated the reversed tropical momentum transports with Rossby waves forced in the tropics, and in particular the horizontal tilts of waves generated as a response to the regions of tropical heating. However, Hartley and Black (1995) found that in their climate model the momentum fluxes on the equator that are equatorward in the northern hemisphere winter were associated with convective outflow rather than Rossby wave propagation and tilted troughs. Also, Zurita-Gotor (2019) -found that the near equatorial momentum transfers were dominated by the correlation of the divergent meridional wind and the rotational zonal wind.

A zonally symmetric and temporally uniform atmosphere and angular momentum conservation in the tropical upper troposphere formed the basis of the simple model of the equinoctial HC given by Held and Hou (1980) in their seminal paper, which followed the study of Schneider (1977). In this model the HCs exist to reduce the mid-tropospheric temperature gradient, and therefore to reduce the upper tropospheric winds implied by thermal wind balance to those which are attainable by angular momentum (AM) conservation from zero zonal wind at the equator. The latitudinal extent of the HC is determined by the latitudinal range over which the reduction of the latitudinal temperature gradient is needed, along with energy conservation. In this model, the sub-tropical jet (STJ) is at the latitude of the edge of the HC and its magnitude is that given by angular momentum conservation. The role of eddies is restricted to removing the discontinuity between this STJ wind and the zero wind in latitudes outside the HC and to reducing the speed of the STJ. A factor of about 3 would be required to give the observed values. The Held and Hou model for an equinoctial HC was extended to include the solsticial seasons by Lindzen and Hou (1988).

Accepted for publication in *Journal of Climate*. DOI 10.1175/JCLI-D-20-0504.1.

A fundamental issue associated with the dynamics of the upper branch of the HC was raised with one of us by John Sawyer (pers. com.) in the 1970s. In a solsticial season, as the air in the upper branch of the HC moves from the tropics of the summer hemisphere to near 30 degrees in the winter hemisphere the change in its potential vorticity (PV) can be expected to be small. Therefore, this air will carry PV of the opposite sign to that of the air in the rest of this winter hemisphere. There is then the possibility of instabilities or a return to the summer hemisphere much as described in the inertial motion discussed by Paldor and Kilworth (1988). Rodwell and Hoskins (1995) found both such behaviours in their study of the low-level inflow to the Indian Summer Monsoon. However, in this contribution to the lower branch of the HC, surface processes were usually found to be able to produce the PV modification that enabled a steady monsoon inflow from the southern Indian Ocean.

In Hoskins et al (2020, hereafter HC1) the dynamics of the HC in June-August (JJA), particularly its upper tropospheric branch, were studied in detail. Zonally averaged momentum and vorticity budgets showed the importance of both steady and transient eddy fluxes. These fluxes had a similar structure to each other in the HC latitudes, with an equatorial maximum and reversal in sign near 12° in the winter (southern) hemisphere. The longitudinal behaviour of the steady and transient fluxes was also found to be similar, and further analysis suggested that they were both associated with motion at the outflow level from a flaring of tropical convection, particularly in the Indian Ocean and W Pacific sectors of the Northern Hemisphere (NH). From the top of these convective regions, filaments of tropical air from the NH moved south-westwards in the upper troposphere across the equator. Some of these filaments returned to the NH and some were mixed in with the ambient air in the southern tropics. However, in strong convective events near 12°S the filaments turned to move south-eastwards and phase in ahead of a trough in the Southern Hemisphere (SH) sub-tropical jet (STJ). The air with its tropical PV values caused a strengthening of the

Accepted for publication in *Journal of Climate*. DOI 10.1175/JCLI-D-20-0504.1.

downstream ridge and the local STJ. In HC1, the temporal and longitudinal variation of the convection and meridional motion was seen to be fundamental in the dynamics of the HC.

In this paper the dynamics of the December to February (DJF) HC are analysed in a manner similar to that used in HC1 for the other solsticial season. The aims of the study are:

- to investigate the similarities and differences between the two seasons
- to determine to what extent this further study reinforces the picture given in HC1-that longitudinal and temporal variations are of order one importance for the HC
- to explore the interaction of the tropics with higher latitudes that is initiated by flaring in regional tropical convection.

Section 2 gives a summary of the equations on which the analysis is based and of the reanalysis data set that is employed. Further details of both are given in HC1. An analysis from a conventional time and zonally averaged perspective is presented in Section 3. Then in Section 4 the time-mean 3-D behaviour is analysed. Section 5 produces a view of the temporal behaviour in terms of spectra and of regressions on OLR in a number of tropical regions. In Section 6 the behaviour through one season is looked at in detail in order to illustrate the synoptic behaviour and to investigate the relevance for it of the regressions in the previous Section. A discussion of the results for the HC in DJF is given in Section 7 and conclusions from this study and that in HC1 for JJA are drawn.

2. Data and diagnostics

The basis for the analysis is ECMWF ERA-Interim re-analysis horizontal winds (u, v), and vorticity fields for the 30-year period from 1981 to 2010. The fields are available 6-hourly with horizontal resolution of about 0.7° and at 37 pressure levels from 1000 to 1 hPa. When fields for a day are shown, the data is averaged over the four periods in the day. In addition, potential vorticity is available on a limited number of isentropic levels, including

Accepted for publication in *Journal of Climate*. DOI 10.1175/JCLI-D-20-0504.1.

350K and 370K. Detailed information on the data can be found in Dee et al. (2011). As a proxy for convection, use is made of NOAA interpolated daily Outgoing Longwave Radiation (OLR) on a 2.5°*2.5° grid (Liebmann and Smith 1996). For part of the analysis and for case studies the single season DJF 2007-8 is used. This season was chosen at random to be the first one to analyse. It is a La Niña year, which will influence the distribution and magnitude of tropical convection, and other years can be expected to show somewhat different detailed behaviour.

It is convenient to use $\mu = \sin\phi$ as latitudinal coordinate, where ϕ is the latitude, and also $U = u\cos\phi$, $V = v\cos\phi$ as velocity variables. The axial component of the specific absolute angular momentum is

$$A = a^2\Omega(1-\mu^2) + aU, \qquad (1)$$

where *a* is the radius of the Earth, and Ω its rotation rate. Denoting a zonal average by [ ] , the zonally averaged equations for *A* and *U* may be written in flux form:

$$\frac{\partial[A]}{\partial t} = a\frac{\partial[U]}{\partial t} = -\frac{\partial}{\partial\mu}[UV] - a\frac{\partial}{\partial p}[\omega U] + af[V] + [F] \ , \qquad (2)$$

where *F* is the frictional force in the longitudinal direction. The derivation of this equation and all the others in this section are discussed in HC1 (Section 2 and the Appendix). As the pressure gradient force impacts on the local rate of change of angular momentum, it is generally more convenient to consider vorticity than angular momentum for analysis of the dynamics in other than a zonally averaged domain. The vertical components of absolute vorticity, ζ, and relative vorticity, ξ, are defined by

$$\zeta = 2\Omega\mu + \xi, \quad \text{and} \quad \xi = \frac{1}{a(1-\mu^2)}\frac{\partial V}{\partial\lambda} - \frac{1}{a}\frac{\partial U}{\partial\mu} \qquad (3)$$

In the zonal average, *A* and ζ are simply related:

$$\frac{1}{a}\frac{\partial[A]}{\partial\mu} = -a\,[\zeta] \qquad (4)$$

In particular, if [*A*] is uniform with latitude then [ζ] is identically zero, a result used by Plumb and Hou (1992) in their discussion of the zonally averaged HC.

Accepted for publication in *Journal of Climate*. DOI 10.1175/JCLI-D-20-0504.1.

The poleward flux of absolute vorticity is:

$$[V\zeta] = \mathrm{f}[V] + [V\xi], \tag{5}$$

and the poleward flux of relative vorticity is related to the momentum flux:

$$[V\xi] = -\frac{1}{a}\frac{\partial}{\partial\mu}[UV] - \left[U\frac{\partial\omega}{\partial p}\right] . \tag{6}$$

Therefore, the angular momentum equation, Eq. (2), can be rewritten using the absolute vorticity flux:

$$\frac{\partial[A]}{\partial t} = a\frac{\partial[U]}{\partial t} = a[V\zeta] - a[\omega\frac{\partial U}{\partial p}] + [F] . \tag{7}$$

In a long-term average the tendency (local time rate of change) terms in Eqs. (2) and (7) will be very small. The terms involving ω are also likely to be small. Away from the boundary layer, the frictional term may be significant in regions of convection, due to convective momentum flux convergence, but is likely to be small elsewhere. Equation (2) emphasises that there must be near balance between the meridional momentum flux convergence and the Coriolis force (terms 1 and 3 in the right-hand expression), and Eq. (7) shows that the poleward absolute vorticity flux must be small compared with its constituent terms.

It will prove useful to make a decomposition of the meridional flux of both U and ξ based on a time average (below this will be for the DJF 30-year period), denoted by an over-bar, and deviations from it by ()′. Then:

$$[\overline{UV}] = [\bar{U}\bar{V}] + [\overline{U'V'}] , \tag{8}$$

$$[\overline{V\zeta}] = f[\bar{V}] + \left[\bar{V}\bar{\xi}\right] + [\overline{V'\xi'}] . \tag{9}$$

In each case, the term involving only products of time-averages will be referred to as the steady flux, and the final term will be referred to as the transient flux.

Use will also be made of the potential vorticity (PV):

$$P = \frac{1}{\rho}\boldsymbol{\zeta}\cdot\boldsymbol{\nabla}\theta \tag{10}$$

Accepted for publication in *Journal of Climate*. DOI 10.1175/JCLI-D-20-0504.1.

where $\boldsymbol{\zeta}$ is the 3-D absolute vorticity. On large length-scales, the term $\frac{1}{\rho}\zeta\frac{\partial\theta}{\partial z}$, involving the vertical component of absolute vorticity, dominates. In the large scale tropics, variation in the absolute vorticity dominates this term so that PV behaviour is mimicked by that of the vertical component of absolute vorticity. Since PV is conserved moving with the atmosphere in the absence of frictional and diabatic processes, away from convective regions it can generally act as a tracer over time-scales of a few days. The inversion properties of PV also mean that implications can be drawn from its distribution for the dynamic and thermodynamic state of the atmosphere (Hoskins et al. 1985).

In Section 5, power spectra of OLR are shown. These are computed over a 120-day time window for each DJF (centred on DJF). A 120-day window is used because a 10% taper (12 days) is applied at the two ends of the data record and to include the intra-seasonal (30-60day) signal. Also in Section 5, regressions are performed on DJF seasonal data. The seasonal trend was not removed as its impact was considered to be negligible for the fields shown.

3. Zonal average perspective

The zonally averaged, time-mean DJF Hadley Cell is shown in Fig.1, with $\mu = \sin\phi$ as the abscissa. In each panel, the meridional circulation is indicated by arrows, representing (V, ω), and the dark blue contours are for the zonal flow, U. The field shown with block colour contours is (a) angular momentum, (b) absolute vorticity and (c) potential vorticity. This figure can be compared with the equivalent for JJA, Fig.1 in HC1. The overturning circulation is to a first approximation the mirror image of that in JJA, with the winter STJ near latitude 30° at the extratropical edge of the HC. However, there are significant departures from this mirror image picture. Whereas the mid-tropospheric ascent region in JJA is concentrated in a peak in the 10° band from 5°N to 15°N, that in DJF is more evenly

Accepted for publication in *Journal of Climate*. DOI 10.1175/JCLI-D-20-0504.1.

distributed in a band 20° wide in the summer hemisphere from 5°N to 15°S. However, the descent occupies a similar range of latitudes in the two winter hemispheres. The Hadley Cell in DJF is distorted in the lower troposphere with the ascent remaining in the NH. As might be expected, this is mainly due to the ITCZs remaining north of the equator in the NH winter.

Zhang et al (2014), in their discussion of shallow meridional circulations in the tropical atmosphere, showed that both shallow and deep Hadley cell modes exist in the two ITCZ regions. In DJF, the low-level flow into the NH, ascent there and the return flow from 800hPa upwards in the ITCZ regions leave their imprint on the zonal average. If the average meridional circulation is calculated for the longitudes other than those of the ITCZs, the picture (not shown) is closer to the mirror image of the zonal mean in JJA, with low level flow into the summer hemisphere (here, SH) and more concentrated mid-tropospheric ascent.

Specific absolute angular momentum, A as defined in Eq. (1) and shown in Fig.1a by block contours, has values near the surface close to that given by the Earth's rotation alone, given the small values of U. There the meridional circulation crosses the contours of A and the frictional term is important in the balance in the momentum/A equation, Eq. (2). In the upper troposphere there is a maximum in A, just north of the equator. There is a sense that the northward motion in the upper branch of the Hadley Cell appears to carry its value of A with it, but there is motion across the contours both in the band from 8°S to the equator and from 5°N to 25°N. Here friction is in general not important and the balance in the momentum equation will be discussed below.

From Eq. (4), the zero absolute vorticity (ζ) contour in Fig. 1b marks the maximum in A. In Fig. 1a it is seen that it remains close to the equator, being slightly north of it in the upper troposphere. The region of small positive ζ extends northward from the equator towards 10°N, consistent with the weak gradient in A there. Potential vorticity (PV, Fig. 1c) shows similar features but also emphasises the high amplitude PV in the stratosphere acting as a lid

Accepted for publication in *Journal of Climate*. DOI 10.1175/JCLI-D-20-0504.1.

on the HC. Also shown in Fig. 1c are some contours of potential temperature. The 350K isentropic surface, near 175hPa, is seen to be close to the maximum flow in the upper branch of the HC, and the 370K-surface, near 100 hPa, towards the upper side of it. The winds and PV on these surfaces will be used for diagnosis in case studies in Section 6.

The steady and transient momentum fluxes for DJF are shown in Fig. 2, which can be compared with the JJA versions (HC1, Fig. 2).The steady flux in the NH is the largest. All these near surface fluxes are associated with the Trade Winds blowing into the ITCZs, in the E Pacific, Atlantic and E Indian Oceans. In JJA, the general picture of these near-surface fluxes was similar, but the steady flux in the SH was slightly larger than that in the NH and the zero-flux line was at about 3°N. The DJF fluxes are consistent with the ITCZs staying near and north of the equator in that season. In the band 0-10°N, the flux convergence is comparable with the Coriolis term in Eq. (2), and their sum is balanced by friction.

In the upper troposphere, the near equatorial maximum in southward momentum fluxes are the equivalent of the rather stronger northward (towards the winter pole) momentum fluxes in JJA (Fig. 2 in HC1). In both seasons, in the tropics the upper tropospheric transient fluxes have a very similar structure in the latitudes of the winter Hadley Cell, though their magnitudes are smaller by a factor of about 2. The steady fluxes were highlighted by Dima and Wallace (2003) and associated by Dima et al (2005) with the tilted troughs of the steady response to tropical heating. However, Zurita-Gotor (2019) stressed the importance of the divergent meridional wind. The smaller transient fluxes appear to have not been discussed explicitly though they were in the figures given by Starr (1970), Rosen and Salstein (1980) and Dima et al (2005).

As expected, there is a large difference in the winter hemisphere fluxes between the two solsticial seasons in the region poleward of the equatorial extremum. In DJF there is a poleward (northward) steady flux maximum of more than 50 $m^2 s^{-2}$ centred at 22°N and a

Accepted for publication in *Journal of Climate*. DOI 10.1175/JCLI-D-20-0504.1.

transient maximum of more than 30 m^2s^{-2} centred at 30°N. However, in JJA the poleward (southward) fluxes in the equivalent region were all associated with the transients, with a maximum of more than 50 $m^2 s^{-2}$.

Referring to the momentum/*A* equation, Eq. (2), the flux divergence from 10°S to the equator balances the Coriolis term associated with the SH portion of the upper branch of the HC, and the convergence from about 3°N to 23°N performs the balance for the NH (winter) portion. It is evident that the near equatorial flux extrema, highlighted previously by Dima and Wallace (2003), play an important role in the momentum budget of the upper branch of the HC in both solsticial seasons.

As discussed above, the form of the *U*/*A* equation in Eq. (7) requires that, in regions of small friction in the upper troposphere, the time-averaged poleward flux of absolute vorticity, $[\overline{V\zeta}]$, must be small compared with its constituent terms. A similar conclusion would be reached by consideration of the vorticity equation at these levels. For DJF 2007-08 and at 200hPa, the flux and its component terms as in Eq. (9) are shown in Fig. 3. From 15°S to 5°N there is little evidence of cancellation in this region of significant deep convection. This is consistent with this being a belt where significant deep convection occurs and the inclusion in the ECMWF system of cumulus momentum transport and the associated friction. However, in the region of the upper branch of the HC north of this, from 5°N to 25°N, both steady and transient fluxes of relative vorticity act to balance the Coriolis term. The steady flux is 3-4 times larger than the transient flux, and the latter is some 50% larger than the residual. In JJA, the cancellation in the region was even greater and the transient flux was slightly more important in the balance. Calculations suggest that the small residual flux is not cancelled by the vertical advection of momentum and a small frictional term would be required for balance even in this region. Alternatively, data assimilation might lead to such a slight imbalance. In passing, we also note the expected higher latitude balance of the Coriolis term, associated

Accepted for publication in *Journal of Climate*. DOI10.1175/JCLI-D-20-0504.1.

with the Ferrel Cell, with the transient flux convergence in the 30°S-50°S band, and with the steady and transient fluxes in the 30°N-50°N band.

In the transient fluxes in the tropics, the contribution from the transient zonal mean terms, i.e. fluctuations in the zonal Hadley Cell are negligible, so that the fluxes are associated almost entirely with the zonally asymmetric, transient eddies. As was the case in JJA (HC1), in both the momentum and vorticity flux views the tropical steady and transient fluxes have a structure that is similar to each other, with the transient flux a factor of 2-3 smaller. The similarity of their structures raises the question whether there is a common mechanism underlying the steady and transient fluxes. The importance of the tropical fluxes in the momentum balance in the upper branch of the winter Hadley Cell contrasts with the view of the complete dominance in it of poleward momentum fluxes associated with the equatorward extension of eddies on and poleward of the winter STJ.

4. 3-D Structure

A picture of the longitudinal structure of the time-mean meridional flow that averages to give the Hadley Cell is provided in Fig. 4 . This presents in a longitude-pressure plane the meridional wind averaged over the 15° latitude band 5°S to 10°N. The picture is robust to the choice of the latitude band, either making it more restricted to the equator or more extended in either hemisphere, apart from in the longitudes of the two ITCZs. The comparable figure for the 10°S to 5°N band in JJA was given in Fig.5 of HC1. Zhang et al (2014) showed similar cross-sections of meridional wind on the equator for January and July.

The basic expectation for the DJF picture is that it is the reverse of that in JJA, with flow into the winter hemisphere (NH) in the upper troposphere and a return in the surface boundary layer. This is the case in the Eastern Hemisphere (EH), over Africa and over the Indian Ocean to the West Pacific, and also over S America, near 300^{o}E (60^{o}W). However, the

Accepted for publication in *Journal of Climate*. DOI10.1175/JCLI-D-20-0504.1.

upper troposphere in the equatorial region of the Western Hemisphere is dominated by two wave trains, one over the Pacific from the date line to 280^{o}E and the other eastwards from S America over the Atlantic to the Greenwich Meridian. The wave-trains appear to propagate eastwards and upwards, and in the case of the Pacific also downwards. The wave-like meridional wind in the equatorial region is the signature of Westward-moving Mixed Rossby Gravity (WMRG) waves. The two regions with the waves are those with westerly winds in the upper tropospheric equatorial region. As shown by, for example, Yang et al. (2007, Fig.7b) and Yang and Hoskins (2016, Fig. 3a), in a westerly basic flow WMRG can be Doppler shifted to have a phase speed that is a reduced westerly or even, for very strong westerlies, zero or eastward . The group velocity is eastward and typically about 20 ms^{-1} so that a wave pattern could develop from 150°W to 60°W in about 4 days. As discussed by Dunkerton and Baldwin (1995), the crest and trough lines tilt in the vertical westwards from the upper tropospheric source level as the waves propagate vertically away from the source level as well as eastwards. The temporal, longitudinal and vertical structures of the waves were shown and discussed in Yang et al. (2011, Figs. 13c, d) and Yang et al. (2012, Figs. 11b, e). The latter showed the WMRG structures for the opposite phases of the QBO, these differing significantly only above 70hPa. Yang and Hoskins (2016, Fig. 6) showed that WMRG activity was present in the E Pacific and Atlantic in both phases of ENSO, though it was stronger in the E Pacific in La Nina and the Atlantic in El Nino, consistent with the differing strength of the westerlies. In Yang and Hoskins (2016, Figs. 10 c, d, and Fig. 12c) it was shown that the westward moving WMRGs in these regions were typically associated with an arching pattern originating in the Southern Hemisphere.

It is proposed here that the waves seen in the upper troposphere can be associated with WMRG waves forced in the E Pacific by convective heating in the South Pacific Convergence Zone (SPCZ) and in the Atlantic by convective heating in S America, south of

Accepted for publication in *Journal of Climate*. DOI 10.1175/JCLI-D-20-0504.1.

the equator. The shorter wavelength of the stationary waves in the Atlantic is consistent with the weaker westerlies there. In JJA, no comparable regions of westerlies are found on the equator, and WMRG waves in the EH are rapidly westward moving synoptic features that are important in triggering convection but leave no signature in the time averaged meridional wind. Further discussion of this is given below.

The geographical distribution of the mean motion at 200 hPa and 950 hPa, and the mean OLR and its standard deviation (SD) are shown in Fig. 5. In Fig. 5b, the dominant regions of convection as indicated are Africa, the Maritime Continent and S America. The low-level north-easterly wind flows into each of these from the neighbouring oceanic regions, and these add up to give most of the low-level branch of the HC. Also apparent are the E Pacific and Atlantic ITCZs, north of the equator with the Trade Winds blowing into them. In the upper troposphere (Fig. 5a), in the EH there is a pair of anticyclones either side of the equator with the strong STJ in the NH and a northward component in the winds from 5°S to 25°N giving much of the upper branch of the HC. There are discrete SH anticylonic circulations over Africa and S America. Equatorial westerlies are present in the E Pacific and Atlantic. The waves on them spread from the SH through the equator, with the shorter wave-length on the weaker westerlies in the Atlantic.

The standard deviation of the OLR is given in Fig. 5c. The Indian Ocean to W Pacific region is implied to have high variability in the region of strong convection. The low latitude portion of the convection in Africa and S America appears to be relatively steady, whereas south and east of these regions there is high variability with moderate intensity convection in the mean. The same also applies in the N Australian region.

Because of their possibly different characteristics, the 12 boxes indicated in Fig.5c have been defined for detailed diagnosis. The details of the 12 regions are indicated in Table 1. The results from most of these will be discussed in the next Section.

Accepted for publication in *Journal of Climate*. DOI10.1175/JCLI-D-20-0504.1.

The final figure of this Section, Fig. 6, shows the 200 hPa longitudinal structure of the momentum fluxes that average zonally to give the fluxes shown in Fig. 2. In HC1 it was found that both the steady and transient fluxes near the equator towards the summer pole and the fluxes in the opposite direction in the winter tropics had major contributions from the EH with more minor ones from the E Pacific and Atlantic sectors. In DJF the major contribution to the tropical fluxes that are important in the winter Hadley Cell, southward near the equator and northward north of this again come from the EH. Referring to Fig. 5a, the steady fluxes are associated with the generally south-easterly winds near the equator, turning to south-westerly in 10°-15°N. The transient fluxes also have a contribution from the E Pacific and Atlantic sectors, but the waves in the mean wind field in the equatorial E Pacific, and to a lesser extent the Atlantic, gives a signature that makes the picture of the steady fluxes more complex. However, as in JJA the major input to the important tropical steady and transient zonally averaged momentum fluxes have a similar structure in longitude as well as latitude, consistent with the possibility of them having a common underlying origin.

5. Temporal behaviour

The first view of the temporal behaviour is provided by Fig. 7 which gives the spectral information for OLR in the 12 boxes shown in Fig. 5c and defined in Table 1. The order of the boxes in Table 1 and Fig. 7 is from Africa eastwards to the Atlantic, with SH boxes directly after their near equatorial counterparts. The period is indicated on the ordinate. In Fig. 7a, the spectral power in each region is given. This highlights the low frequency power, particularly in the EH. To examine the important frequency peaks in each region, Fig. 7b presents the ratio of the spectral power to that associated with a red noise spectrum, with 1 indicating significance at the 95% level. The intra-seasonal time-scale dominates in the near equatorial region from Africa to the Maritime Continent (Boxes 1, 3-5), consistent with the

Accepted for publication in *Journal of Climate*. DOI 10.1175/JCLI-D-20-0504.1.

importance there of the MJO. The 1-2 week period is prominent in SAf (Box 2), and in the off-equatorial boxes for NAus (#6) and the 2-3 week period is prominent in the SPCZ (#8) as it is also in MC (#7). There are peaks in the 4-7 day time-scale in all regions except the MC.

To exhibit the fluctuations in the OLR and in the 200hPa and 950hPa flow and their contribution to the Hadley Cell that are typically associated with variability in OLR in the boxes, two approaches have been taken. In the first, the winds and OLR have been regressed against OLR in each box and the anomalies and full fields for OLR with +/-1.5 standard deviations (SD) have been considered. In the second approach, fields have been composited for the days with the anomaly of OLR averaged over each box exceeding +/- 1.5 SD. The results are very similar and only some of the regression results with OLR set as -1.5 SD will be presented in this paper. In Supplementary Material, as a good summary of anomalies associated with convection in a range of tropical regions, the differences in OLR and 200 hPa wind between the -1.5 SD and +1.5 SD composites are presented for each of the 12 boxes defined in Table 1. The pictures for the regressions with OLR set to +1.5 SD and for the composites for this value of OLR have been used to check the motions when the implied convection in a region is a minimum but will not be commented on explicitly.

The regressions for low OLR, strong convection, in WIO (Box 3) and MC (Box 5) are summarised in Fig. 8. In each panel the block contours show the OLR anomalies and the vectors indicate the full 200 hPa winds. This choice of fields enables the regions of enhanced/reduced convection and the full wind field that accompanies them to be seen. The two regions are chosen to illustrate the MJO behaviour that dominates in the equatorial EH. The OLR anomaly exhibits the anti-phase behaviour between the two regions, with a further anti-phase slightly east of the date-line. The winds in Fig. 8 can be compared with each other and with the 30-year climate in Fig. 5a, and use can be made of the differences in composites shown in Fig. S1c and Fig. S2a . From the region of enhanced convection there is a strong

Accepted for publication in *Journal of Climate*. DOI 10.1175/JCLI-D-20-0504.1.

south-easterly flow across the equator. The direction turns near 10°N to become a strong south-westerly at 20°N and then into the equatorial flank of an enhanced STJ. In the region of supressed convection this flow is much weaker. The tilts and strength of the outflows are consistent with the momentum fluxes (Figs. 2 and 6), southwards near the equator and northwards near 20°N, and are significant contributors to them.

Fig. 9 give the corresponding results for low OLR, active convection, in the off-equatorial regions of SAf (Box 2) and NAus (Box 6), and for SPCZ (Box 8) and SAm (Box 11). Referring first to NAus (Fig. 9b), the anomalous active convection is centred there, but is present in a larger area, including MC. The 200 hPa flow is quite similar to that for MC (Fig. 8b). However, the equatorward flow on the eastern side of the anticyclone over Australia that is associated with the convection over NAus links with the south-easterly flow north of MC to give the possibility of advection from deep in the SH into the enhanced flow into the NH there. Summer seasons with enhanced convection in N Australia have recently been investigated by Sekizawa et al (2018). They noted a teleconnection from there to the region of Japan. This teleconnection is particularly noticeable in Fig. S2b. Anomalies in OLR and flow anomalies are weaker in SAf (Fig. 9a). However, again a link is seen with the flow crossing the equator, this flow being associated with the convection over CAf (Box 1). Figs. S1a and b also show these features. The 150hPa composite flow difference for CAf (not shown) gives a stronger outflow and cross-equatorial flow near 30°E than that at 200hPa.

The patterns of upper tropospheric flow from the two regions of off-equatorial convection seen in Figs. 9a, b are reminiscent of those found in HC1 for JJA, though not as strong as these. In JJA, from active convection in the Indian Ocean/Bay of Bengal and W Pacific/Philippines regions there were north-easterly winds across the equator, turning near 12°S and becoming north-westerly and then turning anticyclonically to merge with the flank of the STJ.

Accepted for publication in *Journal of Climate*. DOI 10.1175/JCLI-D-20-0504.1.

Fig. 9 c, d gives the regression pictures for active convection in the two other main off-equatorial regions of variable active convection, SPCZ and SAm. In the regression, active convection in SPCZ is accompanied by weakened convection in MC (though the reverse link is not seen in Fig. 8b). The 950 hPa motion (not shown) is strongly westerly/north-westerly along the SPCZ, with south-westerlies turning into it on its southern flank. There is evidence of enhanced cross-equatorial flow over the west and central Pacific. The 200 hPa flow turns anticyclonically over the SPCZ to give strong near-equatorial southerlies near 150^{o}W and then north-westerlies near 110^{o}W and weak southerlies near 85^{o}W. This is an enhanced version of the wave-pattern seen in the 30-year average in Fig. 5a, and also in the longitude-pressure cross section in Fig. 4a. Regression of OLR and winds on the equatorial meridional wind near 160^{o}W gives an almost identical wave pattern to the east and an OLR anomaly in the SPCZ region. Figure 9d shows a similar behaviour to that of the SPCZ for strong convection in the S American region. The major difference, as noted before, is the shorter scale of the wave pattern over the Atlantic in the 200 hPa flow. The wave patterns in both regions are clearly seen in the composite differences given in Figs. S2d and S3c.

The E Pacific and Atlantic ITCZ regions (EP-I and Atl-I, Boxes 9 and 12) both give evidence at 200 hPa (see Figs. S3a and d) for the triggering of convection by south-eastward Rossby wave propagation from the extra-tropics. In both cases, the enhanced ITCZ convection is on the equatorial flank of a 200 hPa south-westerly flow anomaly, which is part of the wave train. This wave-train is present through the troposphere (not shown) but tilts slightly backwards (north-westwards) with height, suggesting some baroclinic growth.

In HC1, some regressions were shown for +/-3 day lags with OLR. However, in DJF the general dominance of time-scales 1-2 weeks or longer (except in the ITCZ regions) and, consistent with this, little difference is found if the regressions are lagged by a few days.

Accepted for publication in *Journal of Climate*. DOI 10.1175/JCLI-D-20-0504.1.

6. Examples from 2007-08

To answer the question to what extent the regressions for the 30-year climate are relevant for the fields seen in specific periods, the daily OLR and 350K PV and winds have been looked at for the 2007-08 DJF season. A Hovmöller plot for 200 hPa *v* averaged between 5°S and 10°N is given in Fig. 10 (colours). In the EH slow eastward movement, likely related to the MJO, is seen, together with fast westward moving synoptic systems. In the WH slow moving large-scale waves are present much of the time with varying amplitude. Further evidence that that these are dominated by WMRG waves will be given below.

For discussion here, four days have been selected to represent the behaviour seen in the whole season. All show interesting features associated with enhanced tropical convective activity in one or more of the regions defined in Table 1, and diminished activity in others. The discussion will be organised around these features, rather than on the time development through the period. The days chosen are all from January 2008, apart from 15 February 2008. According to Sekizawa et al. (2018, Fig. 2a), 2007-08 was a weak year for the N Australian summer monsoon, and consistent with this there were no good examples of strong OLR minima there. The February date was added to give another example for active convection in the tropical Australian region.

For the four days, Fig. 11 gives the OLR averages for the specified day and the previous 2 days. The 3-day average for OLR is used to produce a slightly smoother OLR field and because, as seen in HC1, and to take account of the fact that there may be a lag of a day or so before the wind field response away from the active convective region reaches its maximum. Figure 12 shows the PV and winds on the 350 K isentropic surface (about 180 hPa). These will be used to indicate the upper tropospheric motion associated with the variety of convective activity indicated by the OLR. It is worth noting that a 10 m s^{-1} meridional wind would enable an air parcel to move from near the equator to 25°N in about 3 days.

Accepted for publication in *Journal of Climate*. DOI 10.1175/JCLI-D-20-0504.1.

On 1 January and 22 January, convective activity is enhanced over western C Africa and S Africa, with this spreading into the W Indian Ocean on the 22 Jan. On both days there is flow from the S Indian Ocean around the anti-cyclone over S Africa, a south-easterly flow across the equator and into a strong anti-cyclonic perturbation of and strengthening of the NH STJ in the Middle-Eastern region. On 22 Jan, consistent with the convective activity in the WIO, there is south-easterly flow across the equator from there. On 25 Jan (not shown) the active convection region has spread to 80°E and the cross-equatorial south-easterlies are found from Africa to there. On the 16 Jan and 15 Feb, the convection is generally not enhanced over the CAf, SAf and WIO regions, and the flow features noted above are absent or much weaker.

On 1 Jan there is enhanced convective activity in the MC region. Associated with this is a strong anti-cyclone north of it and again a local perturbation and strengthening of the STJ. On 15 Feb the active convection region extends further into Australia and to the east of it. There is now more indication of south-easterly flow from near 20^{o}S and across the equator into the strong NH anticyclone. On 16 and 22 Jan, consistent with the eastward movement of the MJO, convective activity is much weaker than normal, first in the EIO and then in the MC. There is almost zero cross-equatorial flow in the IO and MC regions and the NH anticyclone is weaker, particularly on 22 Jan.

On 16 and 22 Jan there is enhanced convective activity in the SPCZ region, with an eastward shift between the two days. On 16 Jan there is strong southerly flow across the equator near 170^{o}W. 1 Jan had a weaker but similar OLR signature in the region and a similar but weaker flow associated with it. On 22 Jan the cross-equatorial motion is shifted eastwards to nearer 150^{o}W and is a south-easterly. In each case, there are northerlies to the east. The wave pattern moving eastwards along the equator is particularly striking on 16 Jan, with signs of a wave-breaking near S America as the equatorial westerlies weaken.

Accepted for publication in *Journal of Climate*. DOI 10.1175/JCLI-D-20-0504.1.

The Hovmöller plot for 2007-8 of 200 hPa *v* averaged between 5°S and 10°N given in Fig.10 also shows in black line contours *v* obtained by projection of the horizontal structure on to that of the MRG wave, following the methodology of Yang et al. (2003). The similarity with the raw data (Fig 10, block colours) strongly supports the interpretation in terms of WMRG waves. There are slow moving waves in the E Pacific through much of the season, with periods of westward, stationary and eastward phase speed. For much of the time there is evidence of an eastward group velocity of 20 m s^{-1} or more.

The NH anticyclone associated with S American convection is apparent on all four days. The variable convection in the region of S America seen in Fig. 5c and which is partly identified by the SAm box is particularly notable on 22 Jan. In this case there is south-easterly flow around the SH anticyclone and across the equator in the region of enhanced convection and a pronounced anticyclone with northerly flow on its eastward flank.

The four examples shown in Fig.12 are consistent with the more general patterns of the regressions in Figs. 8, and 9, though often stronger than them, as would be expected for individual events. Examples are seen in the 4 days of the MJO enhancement of convection in the WIO to WP summarised in Fig. 8, and also of the diminishment in the opposite phase implied by the regression. The behaviours seen for off-equatorial convection in SAf and NAus seen in these examples are similar to those given in Fig 9a, b, though as remarked above, 2007-08 was a year of generally weak convection in the NAus region. Finally, the triggering of cross-equatorial flow and an eastward wave-pattern by SPCZ and SAm as in Fig. 9c, d was seen in the examples, particularly the SPCZ on 16 Jan. Despite the convection and anomalous flow seen on a daily basis being more localised and flexible in location than the large fixed boxes used in the regressions, it is clear that the flavour of the regression figures are highly relevant to the large-scale behaviour seen on a daily basis.

Accepted for publication in *Journal of Climate*. DOI 10.1175/JCLI-D-20-0504.1.

The strong anticyclones in the NH between the equator and the sub-tropics are seen to be variable in space and time. In the EH they can occur at any longitude, dependent on the phase of the MJO, but are enhanced in the African and MC regions, and in the WH they occur over or to the east of S America. 1 Jan gives good examples of the ones associated with African and MC convection. PV contours show the northward movement of near equatorial or SH PV on its western flank and the southward movement of extratropical PV, and their wrapping up which will lead to irreversible mixing. The signature of this is seen in the southward vorticity and PV flux by the stationary and transient eddies in the NH tropics that was seen to be crucial in the upper branch of the HC (Fig. 3), and its tropical origins are clear. The homogenisation of PV in the regions of the anticyclones is the main contributor to the weak gradients seen in the zonal average in Figs. 1b and c. Equally, the south-easterly flows across the equator, turning to south-westerlies near 12°N are consistent with the momentum fluxes highlighted in the discussion of Fig. 2.

The direct interaction of tropical air flows induced by maxima in regional tropical convective activity with individual mid-latitude weather systems seen in JJA (HC1) has not been seen in our analysis of DJF. However, the direct impact on the behaviour of the NH STJ is clear, and this implies that there will be an impact on the NH extra-tropical weather systems.

Associated with each of the near equatorial active convective events, the enhanced anticyclone in the NH tropics produced a ridge in the NH STJ, an enhancement of its strength and a downstream trough in it. These features are clear for example, in the region of the Red Sea north of the African convection on 1 January (Fig. 12a). They are also seen in the South China region on that day. Three days earlier, on 29 Dec, the Pacific Jet was very short and finished near 140E. During the next 6 days, the jet exit on the eastern side of the anticyclone

Accepted for publication in *Journal of Climate*. DOI 10.1175/JCLI-D-20-0504.1.

extended eastwards as the centre of gravity of the region of tropical convection shifted eastwards until the jet exit reached 150^{o}W on 4 Jan (not shown).

Perhaps the most spectacular extra-tropical interaction seen in 2007-08 was associated with the SPCZ and equatorial E Pacific wave event seen in the 350K PV and flow for 16 Jan (Fig. 12b). This occurred during a 1-2 week period of minimum OLR in the SPCZ box. On 13 Jan (not shown) only the strong cross-equatorial flow near 170^{o}W and the ridge to the east is present. By 16 Jan (Fig.12b) the wave pattern has developed to the east. This is consistent with the eastward group velocity expected for a nearly-stationary WMRG wave on a westerly equatorial flow. According to Fig. 4, the time mean flow suggests propagation upwards as well as eastwards, and such vertical propagation is also expected on theoretical grounds. To investigate this possibility, the PV and winds on the 370K isentropic surface (near 100 hPa) have been looked at during this period, and the fields for 20 Jan are given in Fig. 13a. By 15 Jan wind field anomalies in the E Pacific have started to produce southward and northward perturbations of the near equatorial PV contours. By 18 Jan these features are developing significantly and by 20 Jan (Fig. 13a) filaments of opposite hemisphere air are found deep in each hemisphere. The strong south-westerly flow over Florida and the associated anticyclone over the Caribbean are particularly interesting as they are suggestive of interaction with the middle latitudes. On maps of potential temperature on the PV2 surface (the dynamical tropopause – see e.g. Hoskins, 2015) it is evident that from 20-23 Jan a sharp tropopause gradient progresses from the Florida region to the eastern N Atlantic. These are not shown here, but the resultant change in N Atlantic regime from a jet only near N America to one across the whole N Atlantic is illustrated by the 250 hPa winds for the 2 periods 18-20 and 21-23 Jan (Fig. 13 b, c).

As a final comment in this section, we note that in this season, daily OLR minima in the E Pacific and Atlantic regions are, as expected, found to be associated with the south westerly

Accepted for publication in *Journal of Climate*. DOI 10.1175/JCLI-D-20-0504.1.

motion ahead of the tips of midlatitude troughs as evidenced by the winds and PV. Examples of this for the Pacific are near 15^{o}N, 155^{o}W on 1 Jan and 135^{o}W on 15 Feb and for the Atlantic near 5^{o}N, 30^{o}W on the latter day (Figs. 11 and 12).

7. Discussion

Many aspects of the Hadley Cell in DJF have been seen to be the mirror image of those for JJA previously presented in HC1. However, the Pacific and Atlantic ITCZs stay north of the equator in DJF and the vertical circulations associated with them are somewhat shallower in DJF. These ITCZs act to distort the simple zonally averaged HC reversal picture in the lower troposphere. The upper tropospheric branches of the HC in DJF and JJA are very similar. Angular momentum decreases slower towards the winter pole than implied by the Earth's rotation but is closer to this than it is to a uniform value. Related to this, the magnitude of the absolute vorticity is below that of f, but closer to this than to zero.

In both DJF and JJA, centred close to the equator in the winter hemisphere there is a maximum in the steady and transient fluxes of momentum out of the winter hemisphere, with the steady fluxes being stronger by a factor close to 2. In the two solsticial seasons, the steady and transient fluxes both change sign near 10°-12° in the winter hemisphere. As expected, there are differences at higher latitudes. In DJF the steady poleward fluxes become dominant and have a maximum near 22°N while the transient fluxes becoming larger near 30°N, whereas in the SH winter sub-tropics and extra-tropics the transient fluxes are completely dominant. The constraint that in the upper branch of the HC the poleward flux of absolute vorticity must be small compared with its component terms is achieved in both seasons by the flux of f being largely balanced by the steady and transient fluxes of relative vorticity. Again, both fluxes have a similar structure moving vorticity from the winter tropics to the sub-tropics, with the steady flux being the larger.

Accepted for publication in *Journal of Climate*. DOI10.1175/JCLI-D-20-0504.1.

In JJA the longitudinal structure of the motions that average to give the HC was quite simple, with a dominance in the Indian Ocean to W Pacific region in both the lower and upper branches. This region is again important in DJF, but the African and American signatures are clearer. In the upper troposphere in both the E Pacific and Atlantic regions there is clear evidence of a steady near equatorial wave. The evidence given in this paper suggests that these are WMRG waves, as will be discussed further below. In contrast, in the JJA season, with no such equatorial westerlies, mobile WMRG waves were seen to be important in the triggering of tropical convection (HC1).

As in JJA, the most coherent contribution to the zonally averaged momentum flux were from the E Hemisphere, and again the two fluxes have a similar spatial pattern in this region.

The mean OLR generally emphasises regions closer to the equator than in JJA, when the convective maxima are over southern Asia and the W Pacific near the Philippines. However, the N Australian and SPCZ regions have large temporal variability as well as a significant signature in the mean. This is the case, though to a lesser extent, for S Africa, and S America. The temporal variability in the sector from Africa to the Maritime Continent is more dominated by the intra-seasonal signature of the MJO than in JJA. 1-2 week periods dominate in S Africa and N Australia, and 2-3 weeks dominate in the SPCZ and are important in the MC.

Regressions and composites using 30-year climate data and examples from one season have shown that, associated with active near equatorial convection from Africa to the W Pacific and also S America, the upper tropospheric winds that emanate from the convective regions are south-easterlies in the belt from 0-10°N and turn south-westerly north of this. This is consistent with the equatorward momentum flux south of 10°N and poleward flux north of this. It is also consistent with these signatures being seen in both the steady and transient fluxes. The southerly winds form the western flanks of anticyclones, particularly in

Accepted for publication in *Journal of Climate*. DOI 10.1175/JCLI-D-20-0504.1.

the African, E Asian and S American regions. The anticyclonic motions bring higher latitude air equatorward on their eastern flanks leading to equatorward vorticity fluxes. After active convection the anticyclones will mix air from different latitudes, and therefore act in the sense of local homogenisation of PV and absolute vorticity.

Active off-equatorial convection in the NH in JJA led to filaments of air from the convective regions deep in the summer hemisphere moving across the equator towards the subtropics of the winter hemisphere. This occurs to a lesser extent also in DJF from S Africa , N Australia, the SPCZ and S America. A big difference in DJF is that in this season the latter two are to the west of equatorial westerlies. The flaring of convection in these regions is found to have an associated wave pattern in the equatorial regions of the E Pacific and Atlantic, respectively. It is proposed that these large amplitude waves can be associated with WMRG waves that in a westerly mean flow can be nearly stationary, as well as having large eastward group velocity. The vertical propagation and smaller wavelength in the Atlantic with its weaker westerlies are consistent with the theory of WMRG waves.

The constraint on the dynamics that the time and zonal mean meridional vorticity flux, $[\overline{V\zeta}]$, is small is trivially satisfied in the upper branch of a simple angular momentum conserving HC as ζ is identically zero there. The picture seen here for DJF and in HC1 for JJA is that where and when there is active convection, the strong, confined outflow of air into the winter hemisphere tends to have absolute vorticity more characteristic of equatorial values than the local value of the Coriolis parameter. An assumption of a zero absolute vorticity limit at the tropopause in convective regions in the tropics was used by Emanuel (1995) to derive thermodynamic constraints in the tropics. At other places and times, the contribution to the upper branch of the HC and to $[\overline{V\zeta}]$ is likely to be small. The extreme version of this is the idealised, conceptual model that was given in HC1: convection typically occurs on a proportion α_λ of the longitudes and a proportion α_μ of the time; when and where

Accepted for publication in *Journal of Climate*. DOI 10.1175/JCLI-D-20-0504.1.

there is active convection the meridional flow and the absolute vorticity are, respectively, V and 0, and they are, respectively, 0 and f otherwise. Then $[\overline{V\zeta}] = 0$ so that the dynamical constraint is satisfied. The meridional wind and absolute vorticity in the zonally averaged HC would be αV and $f(1-\alpha)$, where $\alpha = \alpha_\lambda \alpha_\mu$ is the frequency of occurrence of active convection in space and time. The magnitude of the STJ would be αu_{AM}, where u_{AM} is the angular momentum conserving speed. So, for a HC extending to 30° the actual STJ speed would be reduced from 132 ms^{-1} to the observed value of about 40 m s^{-1} if the value of α is about 0.3.

This conceptual model for Hadley Cells is certainly very idealised. However, it is proposed here that, with α in the lower part of the interval 0 to 1, it has advantages as a conceptual model for the HC compared with that based on zonally and temporally uniform overturning with angular momentum conservation (i.e. α = 1). An axisymmetric perspective is retained as useful for analysis, but it is considered that a conceptual model with active convection that is sporadic in space and time may prove to be more useful than one with axisymmetric motion and angular momentum conservation.

As an indication of the relevance of the conceptual model, for one season, DJF 2007/8, Fig. 14 shows the joint pdf at 150 hPa of meridional wind and absolute vorticity in a 10° by 4° box centred on 125°E and 10°N in the outflow region north of the MC. There are indeed signs of a bi-modal distribution, with strong meridional wind (5-11 m s^{-1}) tending to be associated with weak absolute vorticity (0-1.10^{-5} s^{-1}), and of weak meridional wind (0-2 m s^{-1}) associated with larger absolute vorticity (1-2.10^{-5} s^{-1}). For comparison, in the box f is in the range 2-3.10^{-5} s^{-1}. In future work it is intended to further explore the relevance and usefulness of the conceptual model.

One aspect discussed in HC1, with possibly far-reaching implications, was the evidence for a direct interaction between some filaments of near equatorial air triggered by events with active convection in the Indian Ocean and W Pacific sectors and mobile waves on the

Accepted for publication in *Journal of Climate*. DOI10.1175/JCLI-D-20-0504.1.

southern winter STJ. The filaments moved in ahead of a trough in the STJ and appeared to amplify the downstream ridge and the local strength of the STJ. There was also a suggestion that the contribution to the poleward transient eddy momentum flux by these extra-tropical weather systems was enhanced. In DJF the two NH oceanic storm-tracks develop on the STJs that are enhanced by the major upstream convection in the Maritime Continent and S American regions, so that direct interaction of filaments of air from convective outflow with individual weather systems is not likely. However, there is strong evidence for direct effects of motions triggered by tropical convection on the NH STJ and, therefore an expected indirect effect on NH weather systems. Many examples have been given that show that the strong anticyclones north of active convection in the African, East Indian Ocean/W Pacific or S American regions lead to a buckling of the STJ and a local strengthening of it. In 2007-08, an example has also been discussed in which the N Pacific STJ lengthened by 70° as the tropical convection moved eastwards as part of an MJO event. Also in this year, an SPCZ triggered equatorial wave broke near the end of the westerlies in the E Pacific and there was a suggestion that a filament of SH or near equatorial air moved into the N Atlantic and triggered a change of regime from a short to a long jet.

If the conceptual model of the Hadley Cell is adopted, a major question is what determines that, α, the frequency in space and time of active convection is about 0.3 for the Earth's atmosphere. This is the case for both observed solsticial HCs and also for aquaplanet models. Energetic constraints in the tropics, the dynamics and physics of the extra-tropics, in particular the poleward momentum transports, and tropical-extra-tropical interaction like that discussed above are all likely to be important in determining the most realistic value of α.

As in HC1, it is important to question to what extent the ECMWF reanalysis system is able to correctly represent the details in the upper tropospheric response to the flaring of tropical convection, and the shallow filaments of air moving from the tropics of the summer

Accepted for publication in *Journal of Climate*. DOI 10.1175/JCLI-D-20-0504.1.

hemisphere to the tropics and subtropics of the winter hemisphere. However, it seems unlikely that the data will over-emphasise such behaviour.

From the analysis here and in HC1, it is clear that, for a good representation of the tropics in weather and climate models, the systems leading to regional flaring of convection, the level of their outflow, and the representation of shallow filaments of air moving into higher latitudes and interacting with STJ and waves on it would all need to be well represented - a challenge to any weather or climate model. Also, it is likely that any complete theory of the width of the HC and the strength of the STJs and the regional realisation of these will have to take account of the nature of the tropical systems that average to give the HC, and of their rich interactions with the STJ and the extra-tropics.

Acknowledgments We would like to acknowledge the very helpful reviews we received, and in particular that by Thomas Birner. GYY acknowledges the long-term support of the National Centre for Atmospheric Science (NCAS). The research was conducted as part of the NERC project (NE/I012419/1).

Accepted for publication in *Journal of Climate*. DOI 10.1175/JCLI-D-20-0504.1.

References

Davis, N.A, and T. Birner, 2019: Eddy influences on the Hadley Circulation. *J. Mod. Adv. In Earth Systems*, **11**, 1563-1581. https://doi.org/10.1029/2018MS001554

Dee, D. P., and Coauthors, 2011: The ERA-Interim reanalysis: configuration and performance of the data assimilation system. *Quart. J. Roy. Meteor. Soc*., **137**: 553–597.

Dima, I.M., and J.M. Wallace, 2003: On the seasonality of the Hadley cell. *Journal of the Atmospheric Sciences*, **60**, 1522–1527.

Dima, I. M., J. M. Wallace, and I. Kraucunas, 2005: Tropical Zonal Momentum Balance in the NCEP Reanalyses. *J. Atmos. Sci.*, **62**, 2499-513, https://doi.org/10.1175/JAS3486.1.

Dunkerton, T. J., and M. P. Baldwin, 1995: Observation of 3–6-day meridional wind oscillations over the tropical Pacific, 1973–1992: Horizontal structure and propagation. *J. Atmos. Sci*., **52**, 1585–1601.

Eady, E., 1950: The cause of the general circulation of the atmosphere. *Centen. Proc. Roy. Meteor. Soc*., **76**, 156-172.

Emanuel, K. A., 1995: On Thermally Direct Circulations in Moist Atmospheres, *J. Atmos. Sci*., **52**, 1529–1534

Hartley, D.E. and R.X. Black,1995: Mechanistic analysis of interhemispheric transport, *Geophysical Research Letters*, **22**, 2945-2948. https://doi.org/10.1029/95GL02823

Held, I.M., 2018: 100 years of understanding the general circulation of the atmosphere. *Met. Monographs, Amer. Meteor. Soc*., https://doi.org/10.1175/AMSMONOGRAPHS-D-18-0017.1

Held, I.M., and A.Y. Hou, 1980: Nonlinear axially symmetric circulations in a nearly inviscid atmosphere. *Journal of the Atmospheric Sciences*, **37**, 515–533.

Accepted for publication in *Journal of Climate*. DOI 10.1175/JCLI-D-20-0504.1.

Hill, S. A., S. Bordoni, and J. L. Mitchell 2019: Axisymmetric Constraints on Cross-Equatorial Hadley Cell Extent, *J. Atmos. Sci*., **76**, 1547–1564, doi:10.1175/JAS-D-18-0306.1.

Hoskins, B.J., 2015: Potential vorticity and the PV perspective. *Advances in Atmospheric Science*, **32**, 2-9.

Hoskins, B. J., M.E. McIntyre, M.E. and A.W. Robertson, 1985: On the use and significance of isentropic potential vorticity maps. *Quart. J. Roy. Meteor. Soc*.,111, 877–946.

Hoskins, B.J., G.-Y. Yang, and R. M. Fonseca, R. M. 2020. The detailed dynamics of the June-August Hadley cell. *Quart. J. Roy. Meteor. Soc*., **146**, 557-575.

Jeffreys, H. 1926: On the dynamics of the geostrophic winds. *Quart. J. Roy. Meteor. Soc*., **52**, 85-104.

Liebmann, B., and C.A. Smith, 1996: Description of a Complete (Interpolated) outgoing longwave radiation dataset. *Bull. A. Met. Soc*., **77**, 1275-1277.

Lindzen, R. S., and A. V. Hou, 1988: Hadley circulations for zonally averaged heating centered off the equator. *J. Atmos. Sci*., **45**, 2416–2427.

Lorenz, E.N., 1967: The Nature and Theory of the General Circulation of the Atmosphere. World Meteorological Organization Publications, Geneva, Vol. **218**, 161 pp.

Paldor, N., and P.D. Killworth, 1988: Inertial trajectories on a rotating Earth. *J. Atmos. Sci*, **45**, 4013-4019.

Plumb, R.A., and A.Y. Hou, 1992: The Response of a zonally symmetric atmosphere to subtropical thermal forcing: threshold behavior. *J. Atmos. Sci*., **49**, 1790-1799.

Rodwell, M.R., and B.J Hoskins, 1995: A model of the Asian Summer Monsoon II : Cross-equatorial flow and PV behaviour. *J. Atmos. Sci*., **52**, 1341-1356.

Rosen, R.R. and D.A. Salstein, 1980: A comparison between circulation statistics computed from conventional data and NMC Hough analysis. *Mon Wea. Rev*., **108**, 1226-1247.

Accepted for publication in *Journal of Climate*. DOI10.1175/JCLI-D-20-0504.1.

Schneider, E. K. 1977: Axially symmetric steady-state models of the basic state for instability and climate studies. Part II. nonlinear calculations. *J. Atmos. Sci*., **34**, 280–296.

Schneider, T., 2006: The general circulation of the atmosphere. *Reviews of Earth & Planetary Science*, **34**, 655-688.

Sekizawa, S., H. Nakamura, and Y. Kosaka, 2018: Interannual variability of the Australian summer monsoon system internally sustained through wind-evaporation feedback. *Geophysical Research Letters*, **45**. https://doi.org/10.1029/2018GL078536

Simmons, A.J. and Hoskins, B.J., 1978: The life cycles of some non-linear baroclinic waves. *J. Atmos. Sci*., **35**, 414-432.

Starr, V.P., 1948: An essay on the general circulation of the atmosphere. *J. Meteor*., **5**, 39-43.

Starr, V.P., J.P. Peixoto and N.E. Grant, 1970: Momentum and kinetic energy balance of the atmosphere from 5 years of hemispheric data. *Tellus*, **22**, 251-274.

Yang, G-Y., and B.J. Hoskins, 2016 : ENSO-related variation of equatorial MRG and Rossby waves and forcing from higher latitudes. *Quart. J. Roy. Meteor. Soc.* **142**, 1488-2504.

Yang, G-Y., B. J. Hoskins and and L. Gray, 2012: The Influence of the QBO on the propagation of equatorial waves into the stratosphere. *J. Atmos. Sci*., **69**, 2959–2982.

Yang, G-Y., B. J. Hoskins and J. M. Slingo, 2003: Convectively coupled equatorial waves: A new methodology for identifying wave structures in observational data. *J. Atmos. Sci*., **60**, 1637–1654.

Yang, G-Y, Hoskins, B. J., and J.M. Slingo, 2007: Convectively coupled equatorial waves: Part II: Zonal propagation. *J. Atmos. Sci*., **64**, 3424–3437.

Accepted for publication in *Journal of Climate*. DOI 10.1175/JCLI-D-20-0504.1.

Yang, G-Y., B. J. Hoskins and J. M. Slingo, 2011: Equatorial waves in opposite QBO phases**.** *J. Atmos. Sci*., **68**, 839-862

Zhang, C., M. McGauley, and N. A. Bond, 2004: Shallow meridional circulation in the tropical eastern Pacific, *J. Clim.*, **17**, 133– 139.

Zurita-Gotor, P., 2019: The Role of the Divergent Circulation for Large-Scale Eddy Momentum Transport in the Tropics. Part I: Observations. *J. Atmos. Sci*., **76**, 1125–1144, https://doi.org/10.1175/JAS-D-18-0297.1

Accepted for publication in *Journal of Climate*. DOI 10.1175/JCLI-D-20-0504.1.

Table 1 Geographical Regions analysed

#	Geographical Region	Name	Longitude Range	Latitude Range
1	Central Africa	CAf	12ºE-40ºE	5ºN-15ºS
2	Southern Africa	SAf	12ºE -40ºE	15ºS-22ºS
3	Western Indian Ocean	WIO	40ºE -80ºE	0º-20ºS
4	Eastern Indian Ocean	EIO	80ºE -100ºE	10ºN-10ºS
5	Maritime Continent	MC	100ºE -150ºE	10ºN-5ºS
6	Northern Australia & Java	NAus	100ºE -150ºE	5ºS-20ºS
7	Western Pacific	WP	150ºE -180ºE	0º-20ºS
8	South Pacific Convergence Zone	SPCZ	180-130ºW	5ºS-25ºS
9	Eastern Pacific ITCZ	EP-I	145ºW-115ºW	12ºN-5ºN
10	Near-equatorial S America	EqSAm	75ºW-50ºW	5ºN-15ºS
11	Sub-tropical South America	SAm	65ºW-30ºW	15ºS-30ºS
12	Atlantic ITCZ	Atl-I	45ºW-15ºW	10ºN-0º

Accepted for publication in *Journal of Climate*. DOI 10.1175/JCLI-D-20-0504.1.

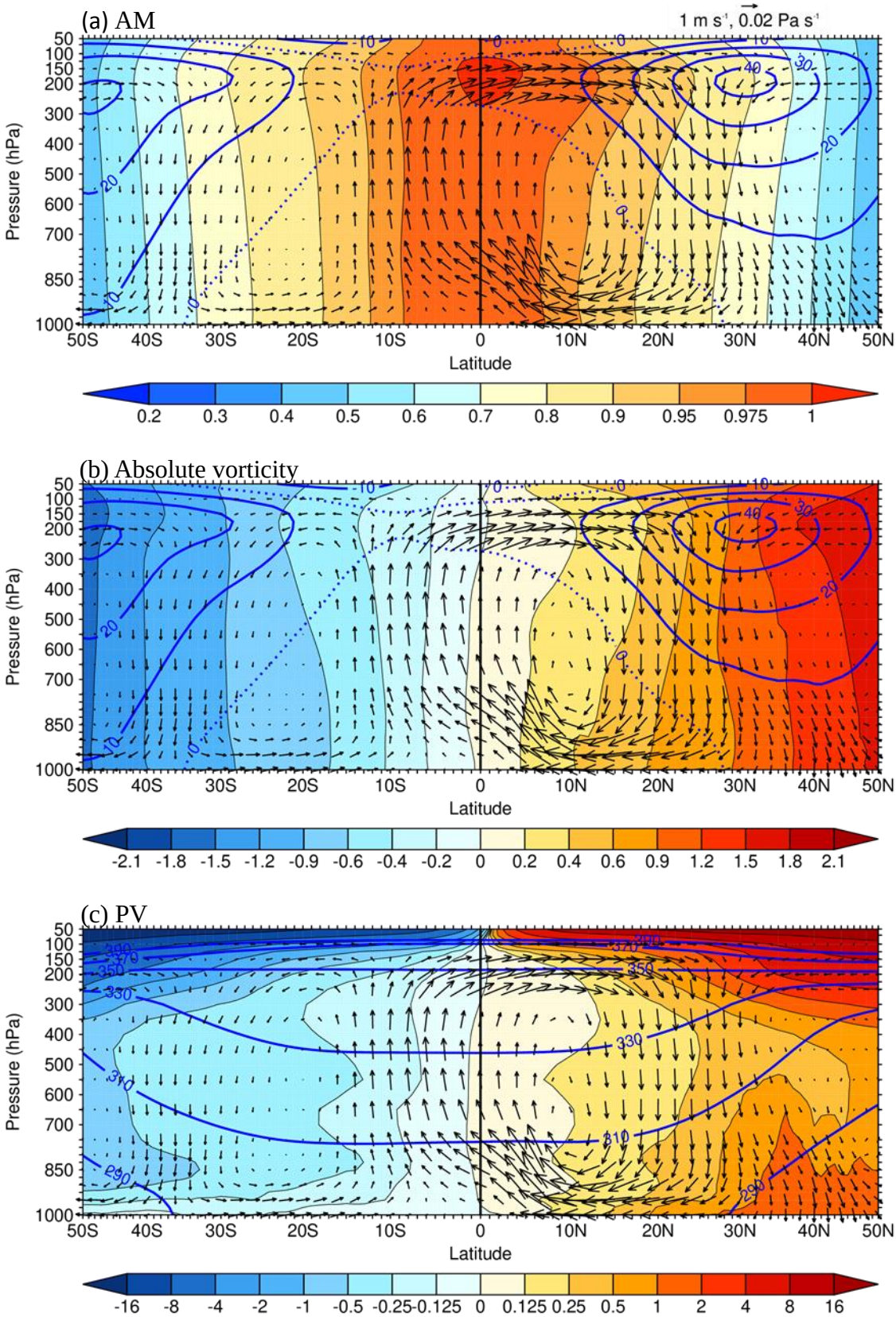

Figure 1. The 30-year mean DJF Hadley Cell. In each panel the meridional circulation (V, ω) is shown by vectors, with the scale at the top right. In the top two panels U is shown by dark blue contours with interval 10 m s^{-1}, and with the zero-contour dotted. In the lower panel the dark blue contours are for the isentropes, with interval 20 K. The abscissa is the sine of the latitude. The fields shown with block contours are: (a) angular momentum (unit $a^2\,\Omega$), (b) the vertical component of absolute vorticity (unit Ω) and (c) potential vorticity (PV) (unit PVU).

Accepted for publication in *Journal of Climate*. DOI 10.1175/JCLI-D-20-0504.1.

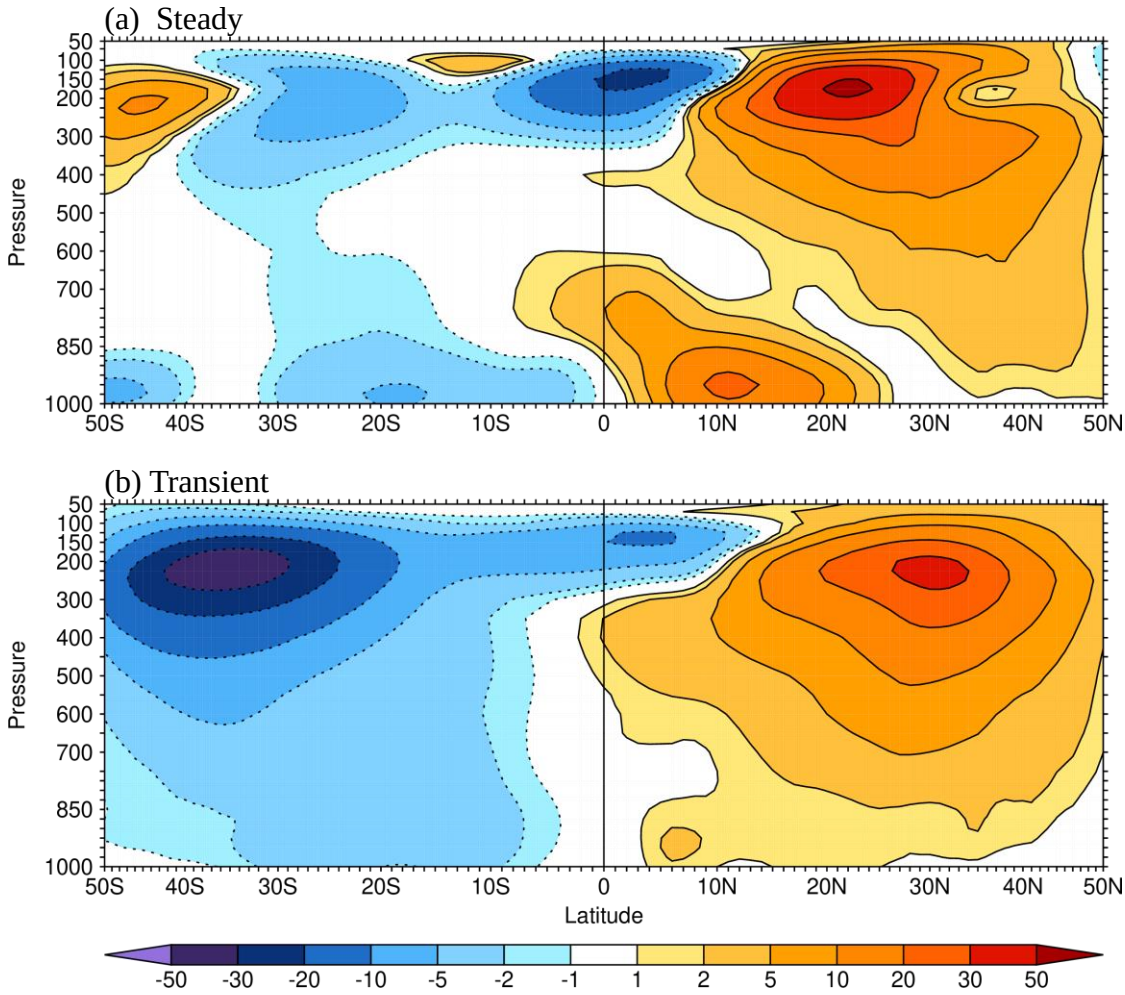

Figure 2 Northward fluxes of angular momentum in 30-year DJF by (a) the steady $[\bar{U}\bar{V}]$ and (b) the transient $\overline{[U'V']}$ motions, as defined in Eq. (8). The contour interval is shown on the colour bar and is not uniform, and contours at negative values are dotted. The unit is $m^2\,s^{-2}$.

Accepted for publication in *Journal of Climate*. DOI 10.1175/JCLI-D-20-0504.1.

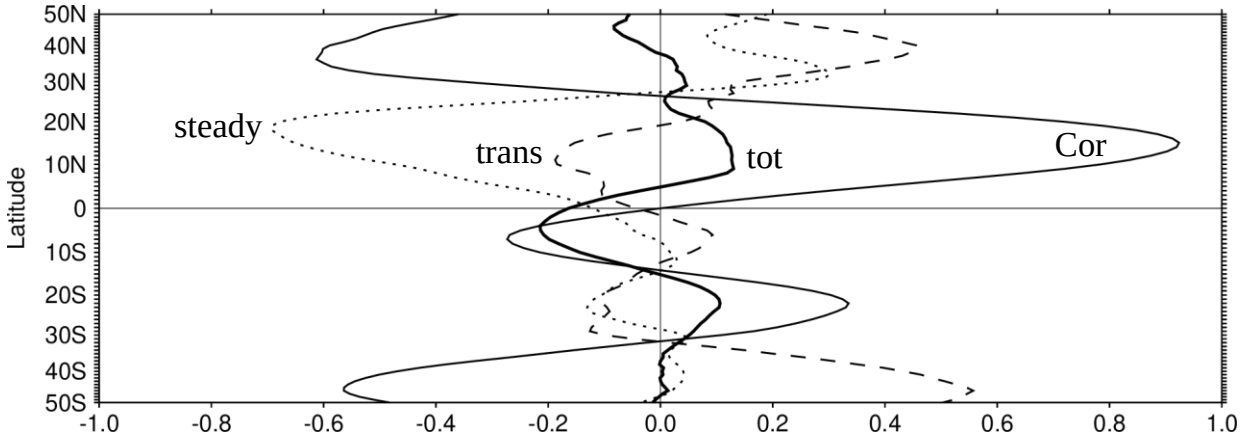

Figure 3 The northward flux of absolute vorticity at 200 hPa for DJF 2007-08, and its component split as in Eq. (9). The total flux is denoted "tot". The three components, the Coriolis torque, the steady flux of relative vorticity and the transient flux are denoted "Cor", "steady" and "trans", respectively. The unit is 1×10^{-4} m s^{-2}. The ordinate is linear in latitude.

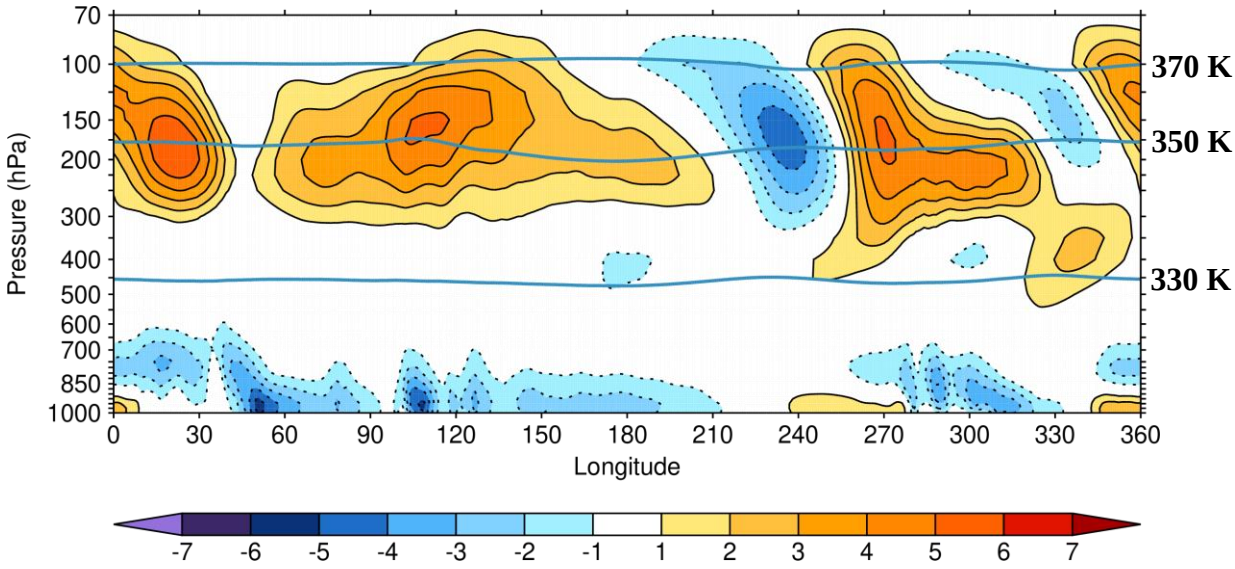

Figure 4 Thirty-year DJF time-mean meridional wind (m s^{-1}) averaged between 5°S and 10°N. Also shown are the isentropic levels 330 K, 350 K and 370 K.

Accepted for publication in *Journal of Climate*. DOI 10.1175/JCLI-D-20-0504.1.

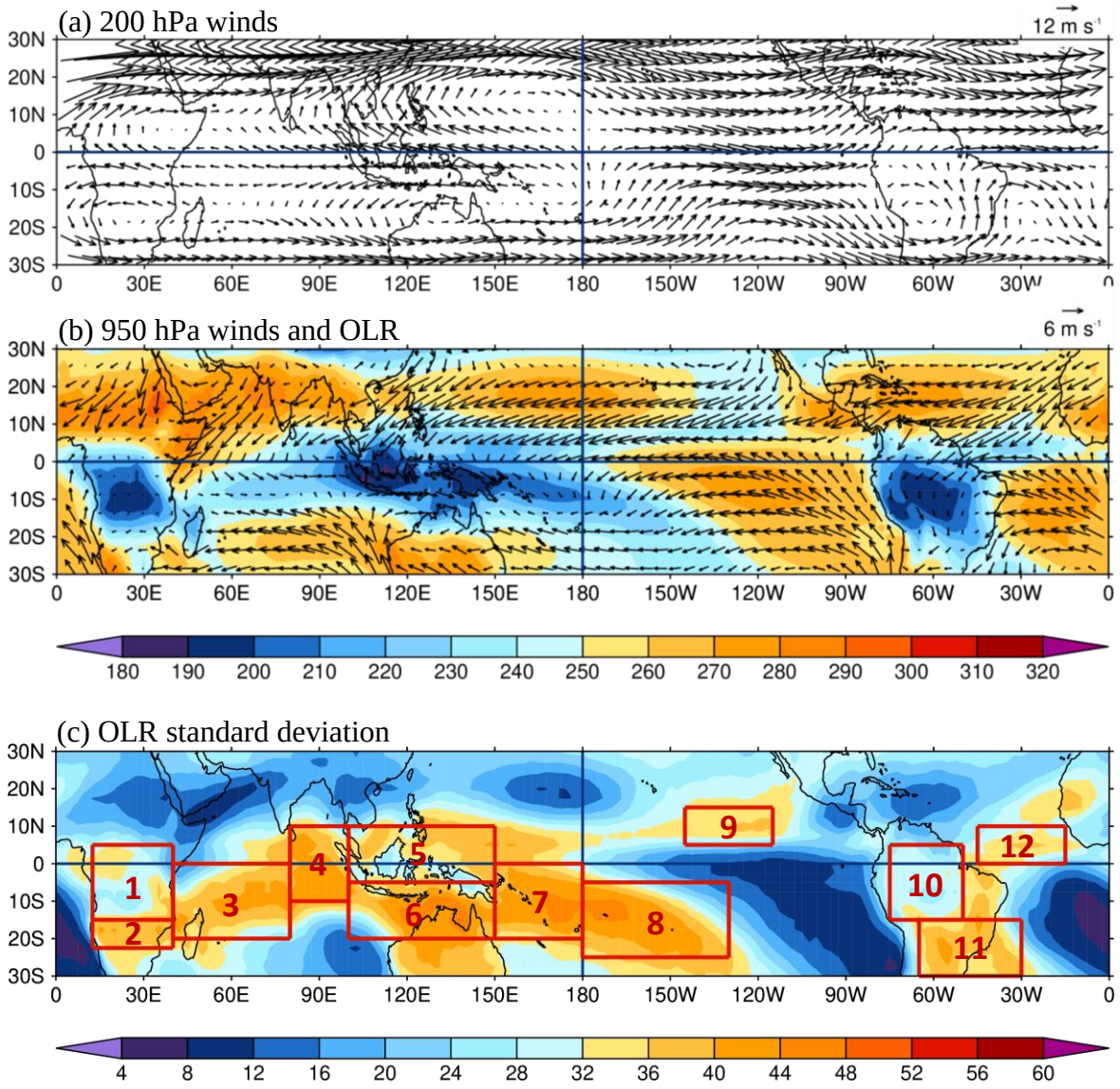

Figure 5 Thirty-year DJF time-mean horizontal winds and OLR statistics. (a) 200hPa vector winds; unit at top right. (b) 950 hPa vector winds (unit at top right) and time-mean OLR (W m^{-2}). (c) Time-mean of the seasonal standard deviation of OLR. The boxes shown in (c) are the 12 regions defined in Table 1.

Accepted for publication in *Journal of Climate*. DOI 10.1175/JCLI-D-20-0504.1.

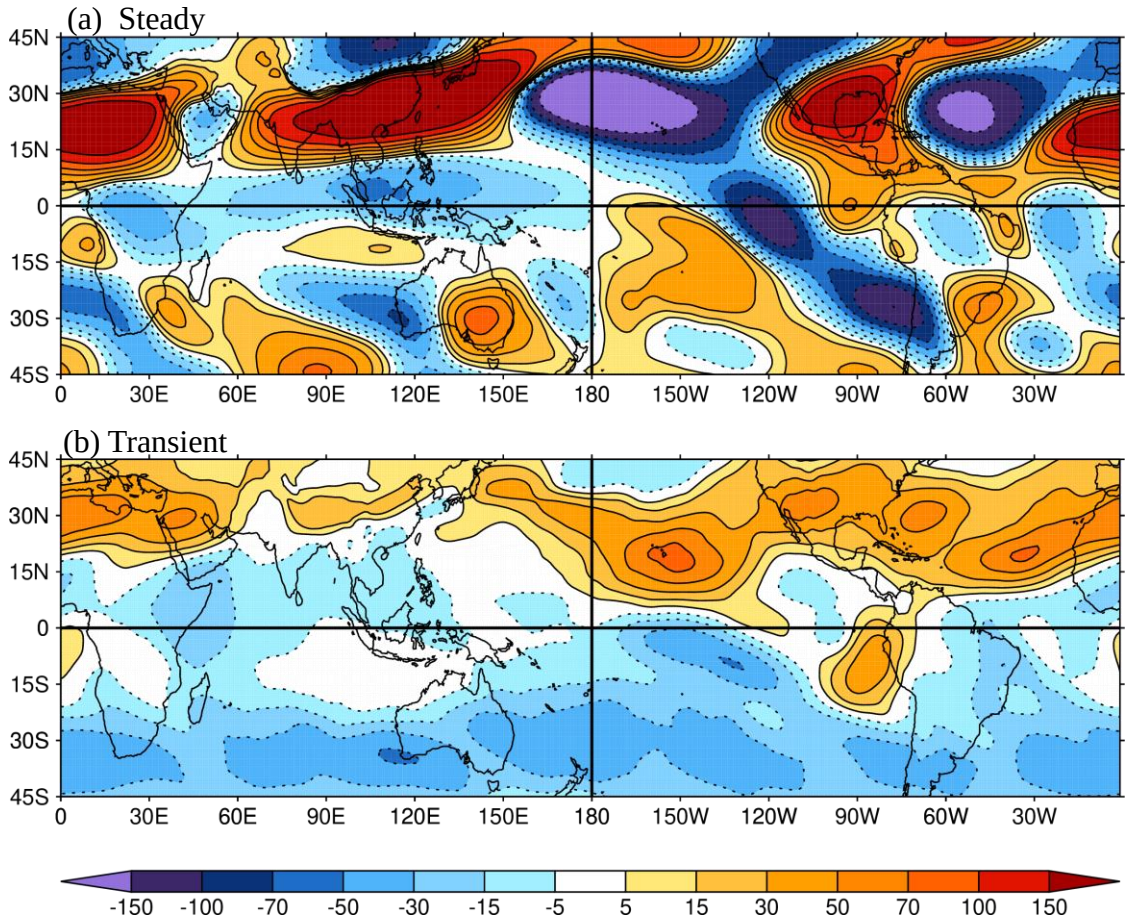

Figure 6 Thirty-year DJF time-mean northward flux of angular momentum at 200 hPa. (a) Steady ($\bar{U}\bar{V}$), and (b) transient ($\overline{U'V'}$). The unit is $m^2 s^{-2}$.

Accepted for publication in *Journal of Climate*. DOI 10.1175/JCLI-D-20-0504.1.

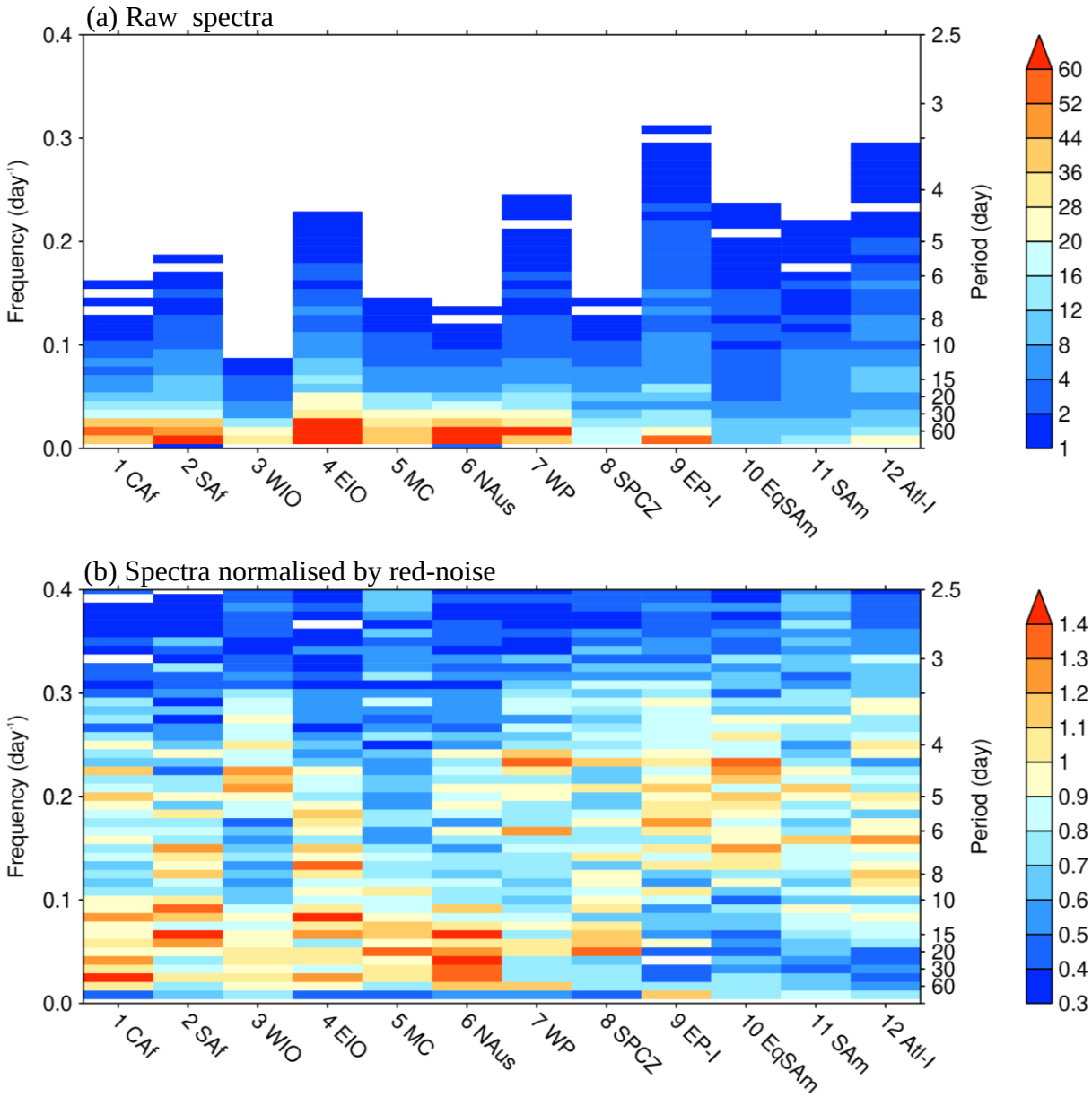

Figure 7 (a) Raw spectra for 30 years of DJF OLR averaged over each of the 12 regions, and (b) spectral power divided by a red-noise power specified with a significance level of 95%, so that values greater than 1 indicate the power exceeding the 95% significance level. The power unit in (a) is $W^2\,m^{-4}$. The regions are as defined in Table 1.

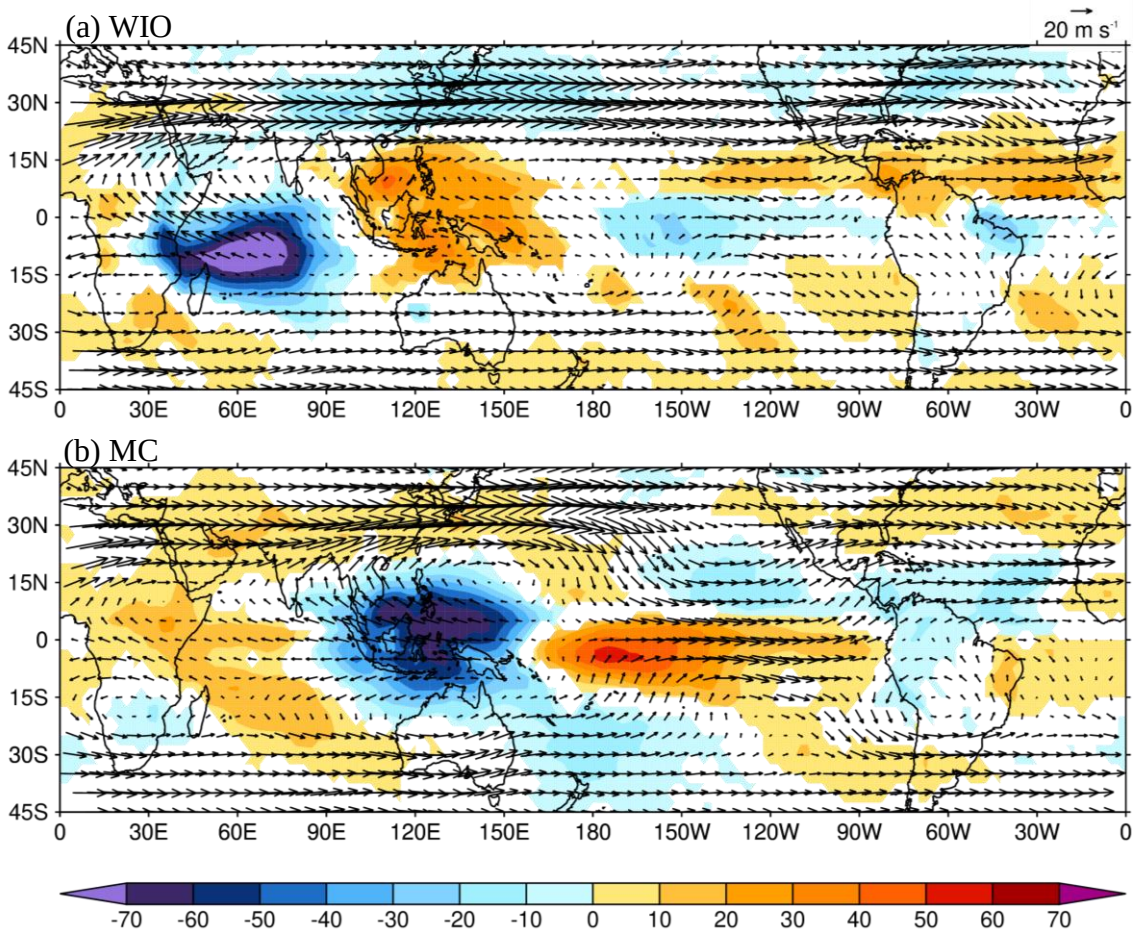

Figure 8 200 hPa horizontal winds (vector) and OLR anomalies (colour) obtained by regressions on OLR averaged over the geographical regions and shown for OLR anomalies in those regions of -1.5 SD. (a) the West Indian Ocean (WIO) and (b) Maritime Continent (MC). The daily data for the regressions is from the 30 years of DJF. The scale for the wind vectors is shown at the top right. The OLR unit is W m^{-2}.

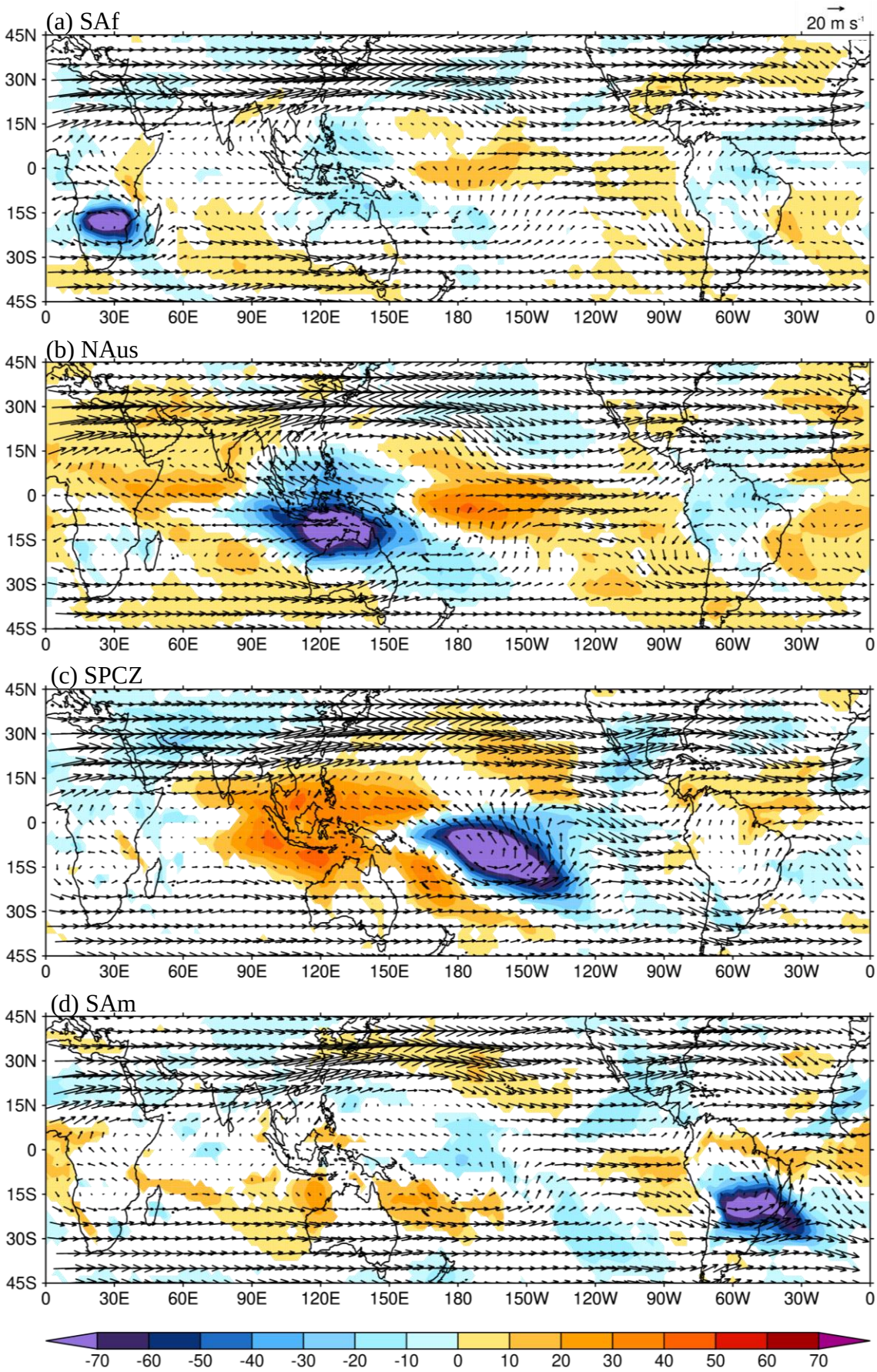

Figure 9 200 hPa horizontal winds (vector) and OLR anomalies (colour) obtained by regressions on OLR averaged over the geographical regions and shown for OLR anomalies in those regions of -1.5 SD. (a) SAf, (b) NAus, (c) SPCZ, and (d) SAm regions. The conventions are as in Fig. 8.

Accepted for publication in *Journal of Climate*. DOI 10.1175/JCLI-D-20-0504.1.

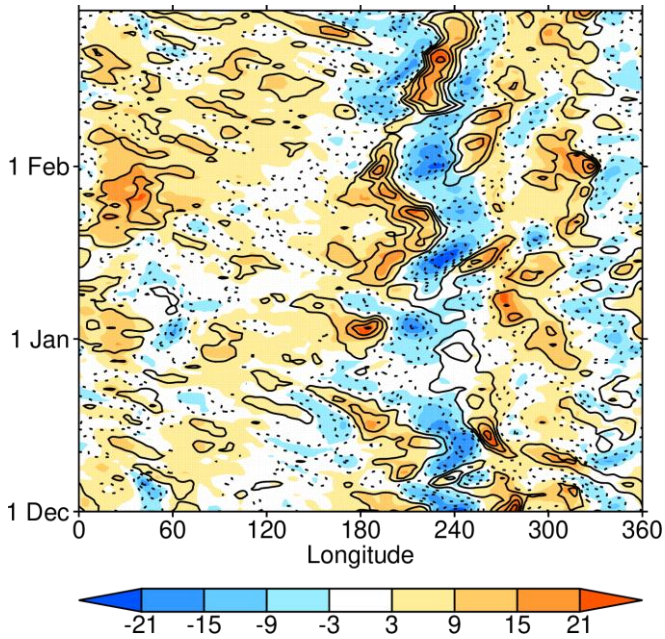

Figure 10 Hovmöller plots of 200 hPa *v* averaged from 5°S to 10°N for DJF 2007-08. The raw data is shown in block colours. The black line contours show the same field but for the projection of the winds and geopotential onto the horizontal structure of the WMRG wave as in Yang et al. (2003), but filtered to leave zonal wavenumbers 2 to 40 and with no time filter. The line contours are at the same values as the change in colours and contours at negative values are dotted.

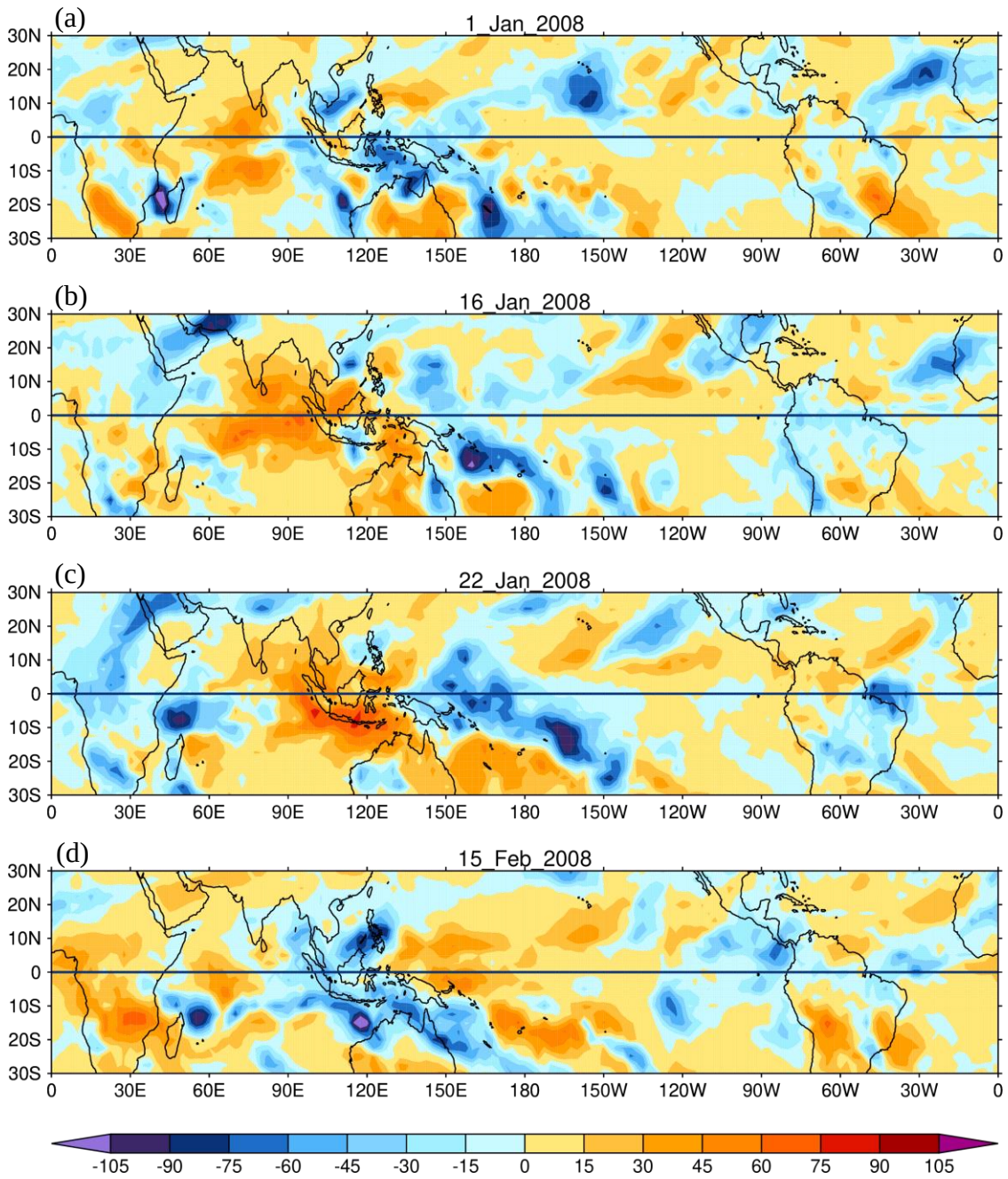

Figure 11 OLR for four days in DJF 2007-08. The OLR is averaged over the specified day and the previous 2 days. The unit for the 3-day OLR average is W m^{-2}.

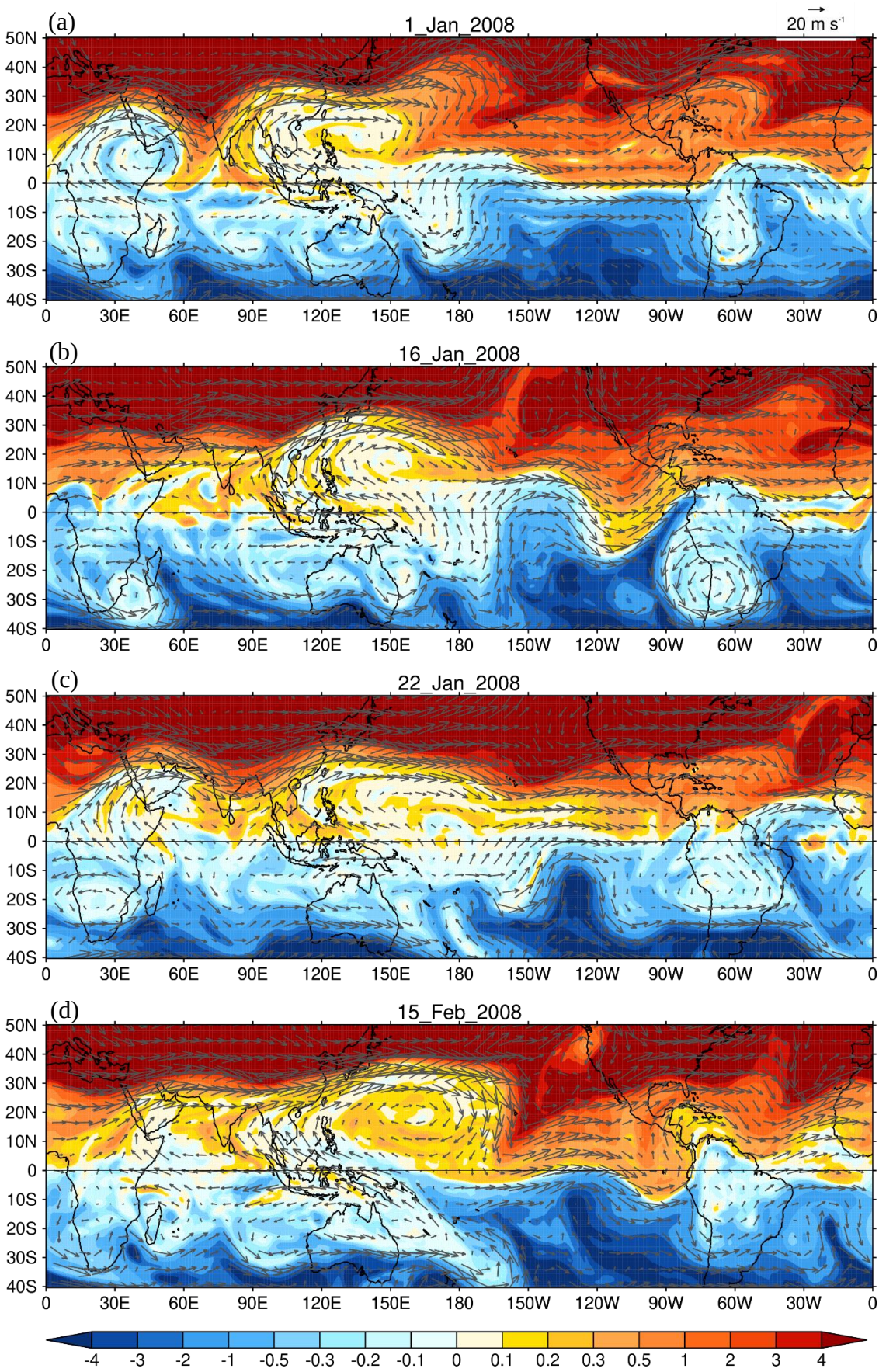

Figure 12 PV (colour) and vector winds on the 350 K isentropic surface for the same four days in the DJF season in 2007-08 as in Fig. 11. The colour bar gives the scale for PV, with unit PVU, and the scale for the winds is shown at the top right.

Accepted for publication in *Journal of Climate*. DOI 10.1175/JCLI-D-20-0504.1.

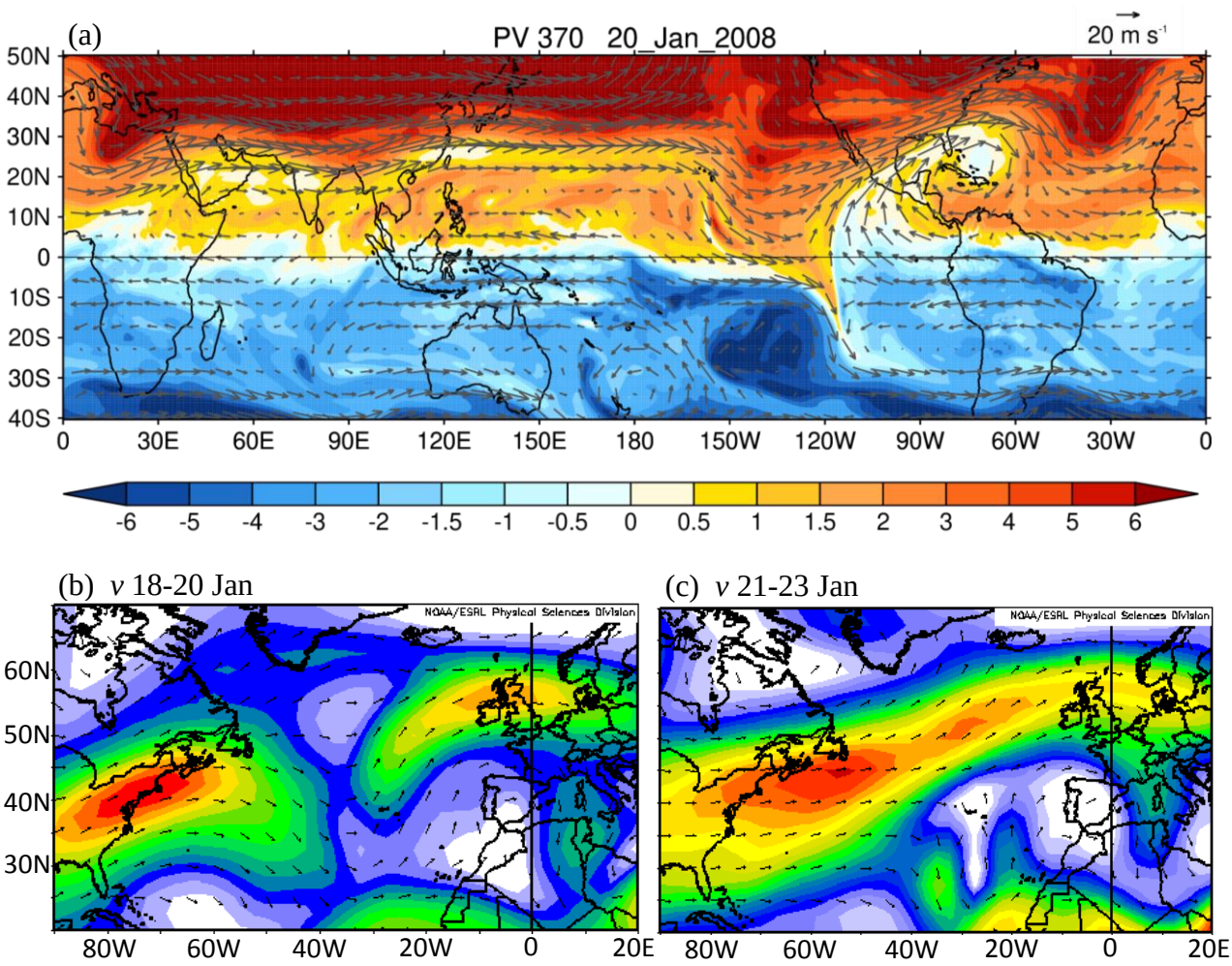

Figure 13 (a) PV (colour) and vector winds on the 370 K isentropic surface on 20 January 2008; the colour bar gives the scale for PV, with unit PVU, and the scale for the winds is shown at the top right. (b) and (c) N Atlantic 250 hPa winds for the periods 18-20 January and 21-23 January 2008; colour shading indicates the magnitude (m s^{-1}) of the wind, and the vectors its direction.

Accepted for publication in *Journal of Climate*. DOI 10.1175/JCLI-D-20-0504.1.

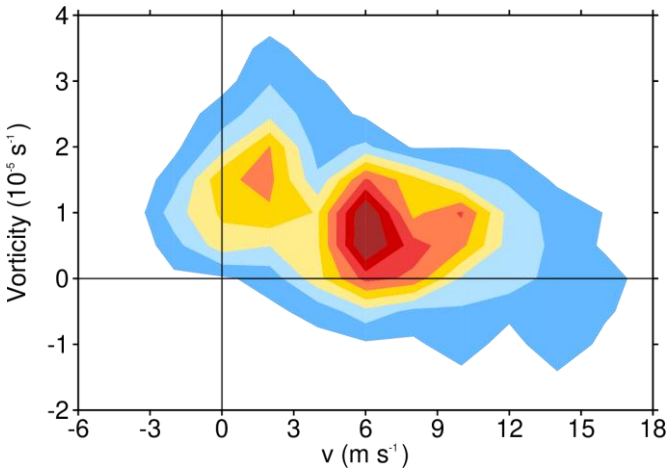

Figure 14 Joint pdf of meridional wind, *v*, (abscissa) and absolute vorticity, ζ, (ordinate) for DJF 2007-08 at 150 hPa in a box 120°E-130°E, 8°N-12°N. The eight contours are at equal intervals.